



**University of
Zurich^{UZH}**

**Zurich Open Repository and
Archive**

University of Zurich
University Library
Strickhofstrasse 39
CH-8057 Zurich
www.zora.uzh.ch

Year: 2011

Measurement of the $B \rightarrow D^{(*)} D^{(*)} K$ branching fractions

BABAR Collaboration ; del Amo Sanchez, P ; Snoek, H L

Abstract: We present a measurement of the branching fractions of the 22 decay channels of the B^0 and B^+ mesons to $D^{(*)} D^{(*)} K$, where the $D^{(*)}$ and $D^{(*)}$ mesons are fully reconstructed. Summing the 10 neutral modes and the 12 charged modes, the branching fractions are found to be $B(B^0 \rightarrow D^{(*)} D^{(*)} K) = (3.68 \pm 0.10 \pm 0.24)\%$ and $B(B^+ \rightarrow D^{(*)} D^{(*)} K) = (4.05 \pm 0.11 \pm 0.28)\%$, where the first uncertainties are statistical and the second systematic. The results are based on 429 fb⁻¹ of data containing 471×10^6 BB pairs collected at the $\Upsilon(4S)$ resonance with the BABAR detector at the SLAC National Accel

DOI: <https://doi.org/10.1103/PhysRevD.83.032004>

Posted at the Zurich Open Repository and Archive, University of Zurich

ZORA URL: <https://doi.org/10.5167/uzh-58695>

Journal Article

Accepted Version

Originally published at:

BABAR Collaboration; del Amo Sanchez, P; Snoek, H L (2011). Measurement of the $B \rightarrow D^{(*)} D^{(*)} K$ branching fractions. *Physical Review D*, 83(3):032004.

DOI: <https://doi.org/10.1103/PhysRevD.83.032004>

Measurement of the $B \rightarrow \bar{D}^{(*)} D^{(*)} K$ branching fractions

P. del Amo Sanchez,¹ J. P. Lees,¹ V. Poireau,¹ E. Prencipe,¹ V. Tisserand,¹ J. Garra Tico,² E. Grauges,² M. Martinelli,^{ab,3} A. Palano,^{ab,3} M. Pappagallo,^{ab,3} G. Eigen,⁴ B. Stugu,⁴ L. Sun,⁴ M. Battaglia,⁵ D. N. Brown,⁵ B. Hooberman,⁵ L. T. Kerth,⁵ Yu. G. Kolomensky,⁵ G. Lynch,⁵ I. L. Osipenkov,⁵ T. Tanabe,⁵ C. M. Hawkes,⁶ A. T. Watson,⁶ H. Koch,⁷ T. Schroeder,⁷ D. J. Asgeirsson,⁸ C. Hearty,⁸ T. S. Mattison,⁸ J. A. McKenna,⁸ A. Khan,⁹ A. Randle-Conde,⁹ V. E. Blinov,¹⁰ A. R. Buzykaev,¹⁰ V. P. Druzhinin,¹⁰ V. B. Golubev,¹⁰ A. P. Onuchin,¹⁰ S. I. Serednyakov,¹⁰ Yu. I. Skovpen,¹⁰ E. P. Solodov,¹⁰ K. Yu. Todyshev,¹⁰ A. N. Yushkov,¹⁰ M. Bondioli,¹¹ S. Curry,¹¹ D. Kirkby,¹¹ A. J. Lankford,¹¹ M. Mandelkern,¹¹ E. C. Martin,¹¹ D. P. Stoker,¹¹ H. Atmacan,¹² J. W. Gary,¹² F. Liu,¹² O. Long,¹² G. M. Vitug,¹² C. Campagnari,¹³ T. M. Hong,¹³ D. Kovalskyi,¹³ J. D. Richman,¹³ C. West,¹³ A. M. Eisner,¹⁴ C. A. Heusch,¹⁴ J. Kroseberg,¹⁴ W. S. Lockman,¹⁴ A. J. Martinez,¹⁴ T. Schalk,¹⁴ B. A. Schumm,¹⁴ A. Seiden,¹⁴ L. O. Winstrom,¹⁴ C. H. Cheng,¹⁵ D. A. Doll,¹⁵ B. Echenard,¹⁵ D. G. Hitlin,¹⁵ P. Ongmongkolkul,¹⁵ F. C. Porter,¹⁵ A. Y. Rakitin,¹⁵ R. Andreassen,¹⁶ M. S. Dubrovin,¹⁶ G. Mancinelli,¹⁶ B. T. Meadows,¹⁶ M. D. Sokoloff,¹⁶ P. C. Bloom,¹⁷ W. T. Ford,¹⁷ A. Gaz,¹⁷ M. Nagel,¹⁷ U. Nauenberg,¹⁷ J. G. Smith,¹⁷ S. R. Wagner,¹⁷ R. Ayad,^{18,*} W. H. Toki,¹⁸ H. Jasper,¹⁹ T. M. Karbach,¹⁹ J. Merkel,¹⁹ A. Petzold,¹⁹ B. Spaan,¹⁹ K. Wacker,¹⁹ M. J. Kobel,²⁰ K. R. Schubert,²⁰ R. Schwierz,²⁰ D. Bernard,²¹ M. Verderi,²¹ P. J. Clark,²² S. Playfer,²² J. E. Watson,²² M. Andreotti,^{ab,23} D. Bettoni,^{a,23} C. Bozzi,^{a,23} R. Calabrese,^{ab,23} A. Cecchi,^{ab,23} G. Cibinetto,^{ab,23} E. Fioravanti,^{ab,23} P. Franchini,^{ab,23} E. Luppi,^{ab,23} M. Munerato,^{ab,23} M. Negrini,^{ab,23} A. Petrella,^{ab,23} L. Piemontese,^{a,23} R. Baldini-Feroli,²⁴ A. Calcaterra,²⁴ R. de Sangro,²⁴ G. Finocchiaro,²⁴ M. Nicolaci,²⁴ S. Pacetti,²⁴ P. Patteri,²⁴ I. M. Peruzzi,^{24,†} M. Piccolo,²⁴ M. Rama,²⁴ A. Zallo,²⁴ R. Contri,^{ab,25} E. Guido,^{ab,25} M. Lo Vetere,^{ab,25} M. R. Monge,^{ab,25} S. Passaggio,^{a,25} C. Patrignani,^{ab,25} E. Robutti,^{a,25} S. Tosi,^{ab,25} B. Bhuyan,²⁶ V. Prasad,²⁶ C. L. Lee,²⁷ M. Morii,²⁷ A. Adametz,²⁸ J. Marks,²⁸ U. Uwer,²⁸ F. U. Bernlochner,²⁹ M. Ebert,²⁹ H. M. Lacker,²⁹ T. Lueck,²⁹ A. Volk,²⁹ P. D. Dauncey,³⁰ M. Tibbetts,³⁰ P. K. Behera,³¹ U. Mallik,³¹ C. Chen,³² J. Cochran,³² H. B. Crawley,³² L. Dong,³² W. T. Meyer,³² S. Prell,³² E. I. Rosenberg,³² A. E. Rubin,³² A. V. Gritsan,³³ Z. J. Guo,³³ N. Arnaud,³⁴ M. Davier,³⁴ D. Derkach,³⁴ J. Firmino da Costa,³⁴ G. Grosdidier,³⁴ F. Le Diberder,³⁴ A. M. Lutz,³⁴ B. Malaescu,³⁴ A. Perez,³⁴ P. Roudeau,³⁴ M. H. Schune,³⁴ J. Serrano,³⁴ V. Sordini,^{34,‡} A. Stocchi,³⁴ L. Wang,³⁴ G. Wormser,³⁴ D. J. Lange,³⁵ D. M. Wright,³⁵ I. Bingham,³⁶ C. A. Chavez,³⁶ J. P. Coleman,³⁶ J. R. Fry,³⁶ E. Gabathuler,³⁶ R. Gamet,³⁶ D. E. Hutchcroft,³⁶ D. J. Payne,³⁶ C. Touramanis,³⁶ A. J. Bevan,³⁷ F. Di Lodovico,³⁷ R. Sacco,³⁷ M. Sigamani,³⁷ G. Cowan,³⁸ S. Paramesvaran,³⁸ A. C. Wren,³⁸ D. N. Brown,³⁹ C. L. Davis,³⁹ A. G. Denig,⁴⁰ M. Fritsch,⁴⁰ W. Gradl,⁴⁰ A. Hafner,⁴⁰ K. E. Alwyn,⁴¹ D. Bailey,⁴¹ R. J. Barlow,⁴¹ G. Jackson,⁴¹ G. D. Lafferty,⁴¹ J. Anderson,⁴² R. Cenci,⁴² A. Jawahery,⁴² D. A. Roberts,⁴² G. Simi,⁴² J. M. Tuggle,⁴² C. Dallapiccola,⁴³ E. Salvati,⁴³ R. Cowan,⁴⁴ D. Dujmic,⁴⁴ G. Sciolla,⁴⁴ M. Zhao,⁴⁴ D. Lindemann,⁴⁵ P. M. Patel,⁴⁵ S. H. Robertson,⁴⁵ M. Schram,⁴⁵ P. Biassoni,^{ab,46} A. Lazzaro,^{ab,46} V. Lombardo,^{a,46} F. Palombo,^{ab,46} S. Stracka,^{ab,46} L. Cremaldi,⁴⁷ R. Godang,^{47,§} R. Kroeger,⁴⁷ P. Sonnek,⁴⁷ D. J. Summers,⁴⁷ X. Nguyen,⁴⁸ M. Simard,⁴⁸ P. Taras,⁴⁸ G. De Nardo,^{ab,49} D. Monorchio,^{ab,49} G. Onorato,^{ab,49} C. Sciacca,^{ab,49} G. Raven,⁵⁰ H. L. Snoek,⁵⁰ C. P. Jessop,⁵¹ K. J. Knoepfel,⁵¹ J. M. LoSecco,⁵¹ W. F. Wang,⁵¹ L. A. Corwin,⁵² K. Honscheid,⁵² R. Kass,⁵² J. P. Morris,⁵² N. L. Blount,⁵³ J. Brau,⁵³ R. Frey,⁵³ O. Igonkina,⁵³ J. A. Kolb,⁵³ R. Rahmat,⁵³ N. B. Sinev,⁵³ D. Strom,⁵³ J. Strube,⁵³ E. Torrence,⁵³ G. Castelli,^{ab,54} E. Feltres,^{ab,54} N. Gagliardi,^{ab,54} M. Margoni,^{ab,54} M. Morandin,^{a,54} M. Posocco,^{a,54} M. Rotondo,^{a,54} F. Simonetto,^{ab,54} R. Stroili,^{ab,54} E. Ben-Haim,⁵⁵ G. R. Bonneaud,⁵⁵ H. Briand,⁵⁵ G. Calderini,⁵⁵ J. Chauveau,⁵⁵ O. Hamon,⁵⁵ Ph. Leruste,⁵⁵ G. Marchiori,⁵⁵ J. Ocariz,⁵⁵ J. Prendki,⁵⁵ S. Sitt,⁵⁵ M. Biasini,^{ab,56} E. Manoni,^{ab,56} A. Rossi,^{ab,56} C. Angelini,^{ab,57} G. Batignani,^{ab,57} S. Bettarini,^{ab,57} M. Carpinelli,^{ab,57,¶} G. Casarosa,^{ab,57} A. Cervelli,^{ab,57} F. Forti,^{ab,57} M. A. Giorgi,^{ab,57} A. Lusiani,^{ac,57} N. Neri,^{ab,57} E. Paoloni,^{ab,57} G. Rizzo,^{ab,57} J. J. Walsh,^{a,57} D. Lopes Pegna,⁵⁸ C. Lu,⁵⁸ J. Olsen,⁵⁸ A. J. S. Smith,⁵⁸ A. V. Telnov,⁵⁸ F. Anulli,^{a,59} E. Baracchini,^{ab,59} G. Cavoto,^{a,59} R. Faccini,^{ab,59} F. Ferrarotto,^{a,59} F. Ferroni,^{ab,59} M. Gaspero,^{ab,59} L. Li Gioi,^{a,59} M. A. Mazzoni,^{a,59} G. Piredda,^{a,59} F. Renga,^{ab,59} T. Hartmann,⁶⁰ T. Leddig,⁶⁰ H. Schröder,⁶⁰ R. Waldi,⁶⁰ T. Adye,⁶¹ B. Franek,⁶¹ E. O. Olaiya,⁶¹ F. F. Wilson,⁶¹ S. Emery,⁶² G. Hamel de Monchenault,⁶² G. Vasseur,⁶² Ch. Yèche,⁶² M. Zito,⁶² M. T. Allen,⁶³ D. Aston,⁶³ D. J. Bard,⁶³ R. Bartoldus,⁶³ J. F. Benitez,⁶³ C. Cartaro,⁶³ M. R. Convery,⁶³ J. Dorfan,⁶³ G. P. Dubois-Felsmann,⁶³ W. Dunwoodie,⁶³ R. C. Field,⁶³ M. Franco Sevilla,⁶³ B. G. Fulsom,⁶³ A. M. Gabareen,⁶³ M. T. Graham,⁶³ P. Grenier,⁶³ C. Hast,⁶³ W. R. Innes,⁶³ M. H. Kelsey,⁶³ H. Kim,⁶³

P. Kim,⁶³ M. L. Kocian,⁶³ D. W. G. S. Leith,⁶³ S. Li,⁶³ B. Lindquist,⁶³ S. Luitz,⁶³ V. Luth,⁶³ H. L. Lynch,⁶³
D. B. MacFarlane,⁶³ H. Marsiske,⁶³ D. R. Muller,⁶³ H. Neal,⁶³ S. Nelson,⁶³ C. P. O'Grady,⁶³ I. Ofte,⁶³
M. Perl,⁶³ T. Pulliam,⁶³ B. N. Ratcliff,⁶³ A. Roodman,⁶³ A. A. Salnikov,⁶³ V. Santoro,⁶³ R. H. Schindler,⁶³
J. Schwiening,⁶³ A. Snyder,⁶³ D. Su,⁶³ M. K. Sullivan,⁶³ S. Sun,⁶³ K. Suzuki,⁶³ J. M. Thompson,⁶³ J. Va'vra,⁶³
A. P. Wagner,⁶³ M. Weaver,⁶³ C. A. West,⁶³ W. J. Wisniewski,⁶³ M. Wittgen,⁶³ D. H. Wright,⁶³ H. W. Wulsin,⁶³
A. K. Yarritu,⁶³ C. C. Young,⁶³ V. Ziegler,⁶³ X. R. Chen,⁶⁴ W. Park,⁶⁴ M. V. Purohit,⁶⁴ R. M. White,⁶⁴
J. R. Wilson,⁶⁴ S. J. Sekula,⁶⁵ M. Bellis,⁶⁶ P. R. Burchat,⁶⁶ A. J. Edwards,⁶⁶ T. S. Miyashita,⁶⁶ S. Ahmed,⁶⁷
M. S. Alam,⁶⁷ J. A. Ernst,⁶⁷ B. Pan,⁶⁷ M. A. Saeed,⁶⁷ S. B. Zain,⁶⁷ N. Guttman,⁶⁸ A. Soffer,⁶⁸ P. Lund,⁶⁹
S. M. Spanier,⁶⁹ R. Eckmann,⁷⁰ J. L. Ritchie,⁷⁰ A. M. Ruland,⁷⁰ C. J. Schilling,⁷⁰ R. F. Schwitters,⁷⁰
B. C. Wray,⁷⁰ J. M. Izen,⁷¹ X. C. Lou,⁷¹ F. Bianchi^{ab,72} D. Gamba^{ab,72} M. Pelliccioni^{ab,72} M. Bomben^{ab,73}
L. Lanceri^{ab,73} L. Vitale^{ab,73} N. Lopez-March,⁷⁴ F. Martinez-Vidal,⁷⁴ D. A. Milanese,⁷⁴ A. Oyanguren,⁷⁴
J. Albert,⁷⁵ Sw. Banerjee,⁷⁵ H. H. F. Choi,⁷⁵ K. Hamano,⁷⁵ G. J. King,⁷⁵ R. Kowalewski,⁷⁵ M. J. Lewczuk,⁷⁵
I. M. Nugent,⁷⁵ J. M. Roney,⁷⁵ R. J. Sobie,⁷⁵ T. J. Gershon,⁷⁶ P. F. Harrison,⁷⁶ T. E. Latham,⁷⁶ E. M. T. Puccio,⁷⁶
H. R. Band,⁷⁷ S. Dasu,⁷⁷ K. T. Flood,⁷⁷ Y. Pan,⁷⁷ R. Prepost,⁷⁷ C. O. Vuosalo,⁷⁷ and S. L. Wu⁷⁷

(The BABAR Collaboration)

¹Laboratoire d'Annecy-le-Vieux de Physique des Particules (LAPP),

Université de Savoie, CNRS/IN2P3, F-74941 Annecy-Le-Vieux, France

²Universitat de Barcelona, Facultat de Física, Departament ECM, E-08028 Barcelona, Spain

³INFN Sezione di Bari^a; Dipartimento di Fisica, Università di Bari^b, I-70126 Bari, Italy

⁴University of Bergen, Institute of Physics, N-5007 Bergen, Norway

⁵Lawrence Berkeley National Laboratory and University of California, Berkeley, California 94720, USA

⁶University of Birmingham, Birmingham, B15 2TT, United Kingdom

⁷Ruhr Universität Bochum, Institut für Experimentalphysik 1, D-44780 Bochum, Germany

⁸University of British Columbia, Vancouver, British Columbia, Canada V6T 1Z1

⁹Brunel University, Uxbridge, Middlesex UB8 3PH, United Kingdom

¹⁰Budker Institute of Nuclear Physics, Novosibirsk 630090, Russia

¹¹University of California at Irvine, Irvine, California 92697, USA

¹²University of California at Riverside, Riverside, California 92521, USA

¹³University of California at Santa Barbara, Santa Barbara, California 93106, USA

¹⁴University of California at Santa Cruz, Institute for Particle Physics, Santa Cruz, California 95064, USA

¹⁵California Institute of Technology, Pasadena, California 91125, USA

¹⁶University of Cincinnati, Cincinnati, Ohio 45221, USA

¹⁷University of Colorado, Boulder, Colorado 80309, USA

¹⁸Colorado State University, Fort Collins, Colorado 80523, USA

¹⁹Technische Universität Dortmund, Fakultät Physik, D-44221 Dortmund, Germany

²⁰Technische Universität Dresden, Institut für Kern- und Teilchenphysik, D-01062 Dresden, Germany

²¹Laboratoire Leprince-Ringuet, CNRS/IN2P3, Ecole Polytechnique, F-91128 Palaiseau, France

²²University of Edinburgh, Edinburgh EH9 3JZ, United Kingdom

²³INFN Sezione di Ferrara^a; Dipartimento di Fisica, Università di Ferrara^b, I-44100 Ferrara, Italy

²⁴INFN Laboratori Nazionali di Frascati, I-00044 Frascati, Italy

²⁵INFN Sezione di Genova^a; Dipartimento di Fisica, Università di Genova^b, I-16146 Genova, Italy

²⁶Indian Institute of Technology Guwahati, Guwahati, Assam, 781 039, India

²⁷Harvard University, Cambridge, Massachusetts 02138, USA

²⁸Universität Heidelberg, Physikalisches Institut, Philosophenweg 12, D-69120 Heidelberg, Germany

²⁹Humboldt-Universität zu Berlin, Institut für Physik, Newtonstr. 15, D-12489 Berlin, Germany

³⁰Imperial College London, London, SW7 2AZ, United Kingdom

³¹University of Iowa, Iowa City, Iowa 52242, USA

³²Iowa State University, Ames, Iowa 50011-3160, USA

³³Johns Hopkins University, Baltimore, Maryland 21218, USA

³⁴Laboratoire de l'Accélérateur Linéaire, IN2P3/CNRS et Université Paris-Sud 11,
Centre Scientifique d'Orsay, B. P. 34, F-91898 Orsay Cedex, France

³⁵Lawrence Livermore National Laboratory, Livermore, California 94550, USA

³⁶University of Liverpool, Liverpool L69 7ZE, United Kingdom

³⁷Queen Mary, University of London, London, E1 4NS, United Kingdom

³⁸University of London, Royal Holloway and Bedford New College, Egham, Surrey TW20 0EX, United Kingdom

³⁹University of Louisville, Louisville, Kentucky 40292, USA

⁴⁰Johannes Gutenberg-Universität Mainz, Institut für Kernphysik, D-55099 Mainz, Germany

⁴¹University of Manchester, Manchester M13 9PL, United Kingdom

⁴²University of Maryland, College Park, Maryland 20742, USA

⁴³University of Massachusetts, Amherst, Massachusetts 01003, USA

- ⁴⁴Massachusetts Institute of Technology, Laboratory for Nuclear Science, Cambridge, Massachusetts 02139, USA
⁴⁵McGill University, Montréal, Québec, Canada H3A 2T8
⁴⁶INFN Sezione di Milano^a; Dipartimento di Fisica, Università di Milano^b, I-20133 Milano, Italy
⁴⁷University of Mississippi, University, Mississippi 38677, USA
⁴⁸Université de Montréal, Physique des Particules, Montréal, Québec, Canada H3C 3J7
⁴⁹INFN Sezione di Napoli^a; Dipartimento di Scienze Fisiche, Università di Napoli Federico II^b, I-80126 Napoli, Italy
⁵⁰NIKHEF, National Institute for Nuclear Physics and High Energy Physics, NL-1009 DB Amsterdam, The Netherlands
⁵¹University of Notre Dame, Notre Dame, Indiana 46556, USA
⁵²Ohio State University, Columbus, Ohio 43210, USA
⁵³University of Oregon, Eugene, Oregon 97403, USA
⁵⁴INFN Sezione di Padova^a; Dipartimento di Fisica, Università di Padova^b, I-35131 Padova, Italy
⁵⁵Laboratoire de Physique Nucléaire et de Hautes Energies, IN2P3/CNRS, Université Pierre et Marie Curie-Paris6, Université Denis Diderot-Paris7, F-75252 Paris, France
⁵⁶INFN Sezione di Perugia^a; Dipartimento di Fisica, Università di Perugia^b, I-06100 Perugia, Italy
⁵⁷INFN Sezione di Pisa^a; Dipartimento di Fisica, Università di Pisa^b; Scuola Normale Superiore di Pisa^c, I-56127 Pisa, Italy
⁵⁸Princeton University, Princeton, New Jersey 08544, USA
⁵⁹INFN Sezione di Roma^a; Dipartimento di Fisica, Università di Roma La Sapienza^b, I-00185 Roma, Italy
⁶⁰Universität Rostock, D-18051 Rostock, Germany
⁶¹Rutherford Appleton Laboratory, Chilton, Didcot, Oxon, OX11 0QX, United Kingdom
⁶²CEA, Irfu, SPP, Centre de Saclay, F-91191 Gif-sur-Yvette, France
⁶³SLAC National Accelerator Laboratory, Stanford, California 94309 USA
⁶⁴University of South Carolina, Columbia, South Carolina 29208, USA
⁶⁵Southern Methodist University, Dallas, Texas 75275, USA
⁶⁶Stanford University, Stanford, California 94305-4060, USA
⁶⁷State University of New York, Albany, New York 12222, USA
⁶⁸Tel Aviv University, School of Physics and Astronomy, Tel Aviv, 69978, Israel
⁶⁹University of Tennessee, Knoxville, Tennessee 37996, USA
⁷⁰University of Texas at Austin, Austin, Texas 78712, USA
⁷¹University of Texas at Dallas, Richardson, Texas 75083, USA
⁷²INFN Sezione di Torino^a; Dipartimento di Fisica Sperimentale, Università di Torino^b, I-10125 Torino, Italy
⁷³INFN Sezione di Trieste^a; Dipartimento di Fisica, Università di Trieste^b, I-34127 Trieste, Italy
⁷⁴IFIC, Universitat de Valencia-CSIC, E-46071 Valencia, Spain
⁷⁵University of Victoria, Victoria, British Columbia, Canada V8W 3P6
⁷⁶Department of Physics, University of Warwick, Coventry CV4 7AL, United Kingdom
⁷⁷University of Wisconsin, Madison, Wisconsin 53706, USA

(Dated: November 18, 2010)

We present a measurement of the branching fractions of the 22 decay channels of the B^0 and B^+ mesons to $\bar{D}^{(*)}D^{(*)}K$, where the $D^{(*)}$ and $\bar{D}^{(*)}$ mesons are fully reconstructed. Summing the 10 neutral modes and the 12 charged modes, the branching fractions are found to be $\mathcal{B}(B^0 \rightarrow \bar{D}^{(*)}D^{(*)}K) = (3.68 \pm 0.10 \pm 0.24)\%$ and $\mathcal{B}(B^+ \rightarrow \bar{D}^{(*)}D^{(*)}K) = (4.05 \pm 0.11 \pm 0.28)\%$, where the first uncertainties are statistical and the second systematic. The results are based on 429 fb^{-1} of data containing $471 \times 10^6 B\bar{B}$ pairs collected at the $\Upsilon(4S)$ resonance with the BABAR detector at the SLAC National Accelerator Laboratory.

PACS numbers: 13.25.Hw, 14.40.Nd

I. INTRODUCTION

In this article, we report on the measurement of the branching fractions of the 22 decays of charged and neutral B mesons to $\bar{D}^{(*)}D^{(*)}K$ final states (Table I): $D^{(*)}$ is either a D^0 , D^{*0} , D^+ or D^{*+} , $\bar{D}^{(*)}$ is the charge conjugate of $D^{(*)}$ and K is either a K^+ or a K^0 . Both $\bar{D}^{(*)}$ and $D^{(*)}$ are fully reconstructed. Charge conjugate reactions are assumed throughout this article.

In the past, the values measured for hadronic decays of the B meson were in disagreement with the expec-

*Now at Temple University, Philadelphia, Pennsylvania 19122, USA

†Also with Università di Perugia, Dipartimento di Fisica, Perugia, Italy

‡Also with Università di Roma La Sapienza, I-00185 Roma, Italy

§Now at University of South Alabama, Mobile, Alabama 36688, USA

¶Also with Università di Sassari, Sassari, Italy

tations based on the B semileptonic branching fraction due to the inconsistency originating from the number of charmed hadrons per B decay (charm counting) [1]. The $b \rightarrow c\bar{c}s$ transition in B decays was believed to be dominated by $B \rightarrow D_s X$, $B \rightarrow (c\bar{c})X$, and $B \rightarrow \Xi_c X$ final states, where X represents any particles. However, it was realized [2] that an enhancement in the $b \rightarrow c\bar{c}s$ transition was needed to resolve the theoretical discrepancy with the B semileptonic branching fraction. Buchalla *et al.* [2] predicted sizeable branching fractions for decays of the form $B \rightarrow \bar{D}^{(*)}D^{(*)}K(X)$. Experimental evidence in support of this picture soon appeared in the literature [3], including a study by *BABAR* using 76 fb^{-1} of data where the Collaboration reported the observations or the limits on the 22 decays $B \rightarrow \bar{D}^{(*)}D^{(*)}K$ [4]. The aggregate branching fraction measurements were $\mathcal{B}(B^0 \rightarrow \bar{D}^{(*)}D^{(*)}K) = (4.3 \pm 0.3 \pm 0.6)\%$ and $\mathcal{B}(B^+ \rightarrow \bar{D}^{(*)}D^{(*)}K) = (3.5 \pm 0.3 \pm 0.5)\%$, where the first uncertainties are statistical and the second systematic. This result may be compared with the wrong-sign D production ($b \rightarrow c\bar{c}s$ transition containing a \bar{D} meson) that *BABAR* studied using inclusive B decays to final states containing at least one charm particle [5]. The wrong-sign D production was found to be $\mathcal{B}(\bar{B}^0 \rightarrow \bar{D}X) = (10.4 \pm 1.9)\%$ and $\mathcal{B}(B^- \rightarrow \bar{D}X) = (11.1 \pm 0.9)\%$. In addition, *BABAR* found a value of the total charm yield per B decay consistent with the one derived from the semileptonic branching fraction, which solved the long-standing problem of the charm counting.

Furthermore, $\bar{D}^{(*)}D^{(*)}K$ events are interesting for a variety of studies. These events can be used to investigate isospin relations and to extract a measurement of the ratio of $\Upsilon(4S) \rightarrow B^+B^-$ and $\Upsilon(4S) \rightarrow B^0\bar{B}^0$ decays [6]. It was shown theoretically that the time-dependent rate for $B^0 \rightarrow D^{(*)-}D^{(*)+}K_s^0$ decays can be used to measure $\sin 2\beta$ and $\cos 2\beta$ [7]. *BABAR* used the mode $B^0 \rightarrow D^{*-}D^{*+}K_s^0$ with 209 fb^{-1} of data to perform a time-dependent CP asymmetry measurement to determine the sign of $\cos 2\beta$ [8]. The Belle Collaboration also published a similar analysis [9]. Although the resonant states are not studied in our paper, it is worth recalling that many $D^{(*)}K$ and $\bar{D}^{(*)}D^{(*)}$ resonant processes are at play in the studied decay channels. Using $B \rightarrow \bar{D}^{(*)}D^{(*)}K$ final states, *BABAR* and Belle observed and measured the properties of the resonances D_{s1}^+ (2536), D_{sJ} (2700), ψ (3770), and X (3872) [10–12].

The $B \rightarrow \bar{D}^{(*)}D^{(*)}K$ decays can proceed through external W -emission and internal W -emission amplitudes, also called color-suppressed amplitudes. As Fig. 1 illustrates, some decay modes proceed through only one of these amplitudes while others proceed through both.

In this paper, we update with the full *BABAR* data sample our previous measurement [4] of the branching fractions for the 22 $B \rightarrow \bar{D}^{(*)}D^{(*)}K^0$ and $B \rightarrow \bar{D}^{(*)}D^{(*)}K^+$ decays. We benefit from several improvements with respect to this previous measurement:

- the integrated luminosity used for this analysis is more than five times larger,

- the track reconstruction and particle identification algorithms have been improved (in purity and efficiency),
- the efficiency of the selection of signal events has been increased,
- the fit uses a more accurate signal parametrization,
- the peaking background is taken into account in the fit,
- we use a method that is insensitive to the possible resonant structure in the final states.

Measuring the 22 modes altogether allows to avoid biases in the branching fraction measurement by correctly taking into account the cross-feed events, which are events from one mode being reconstructed as a candidate for another mode.

TABLE I: The 22 $B \rightarrow \bar{D}^{(*)}D^{(*)}K$ decay modes. The modes $B^0 \rightarrow D^-D^{*+}K^0$ and $B^0 \rightarrow D^{*-}D^+K^0$ are combined together since they are not experimentally distinguishable. The same applies to the modes $B^0 \rightarrow \bar{D}^0D^{*0}K^0$ and $B^0 \rightarrow \bar{D}^{*0}D^0K^0$ which are also combined together.

Neutral B mode	Charged B mode
$B^0 \rightarrow D^-D^0K^+$	$B^+ \rightarrow \bar{D}^0D^+K^0$
$B^0 \rightarrow D^-D^{*0}K^+$	$B^+ \rightarrow \bar{D}^0D^{*+}K^0$
$B^0 \rightarrow D^{*-}D^0K^+$	$B^+ \rightarrow \bar{D}^{*0}D^+K^0$
$B^0 \rightarrow D^{*-}D^{*0}K^+$	$B^+ \rightarrow \bar{D}^{*0}D^{*+}K^0$
$B^0 \rightarrow D^-D^+K^0$	$B^+ \rightarrow \bar{D}^0D^0K^+$
$B^0 \rightarrow D^-D^{*+}K^0 + D^{*-}D^+K^0$	$B^+ \rightarrow \bar{D}^0D^{*0}K^+$
	$B^+ \rightarrow \bar{D}^{*0}D^0K^+$
$B^0 \rightarrow D^{*-}D^{*+}K^0$	$B^+ \rightarrow \bar{D}^{*0}D^{*0}K^+$
$B^0 \rightarrow \bar{D}^0D^0K^0$	$B^+ \rightarrow D^-D^+K^+$
$B^0 \rightarrow \bar{D}^0D^{*0}K^0 + \bar{D}^{*0}D^0K^0$	$B^+ \rightarrow D^-D^{*+}K^+$
	$B^+ \rightarrow D^{*-}D^+K^+$
$B^0 \rightarrow \bar{D}^{*0}D^{*0}K^0$	$B^+ \rightarrow D^{*-}D^{*+}K^+$

II. THE *BABAR* DETECTOR AND DATA SAMPLE

The data were recorded by the *BABAR* detector at the PEP-II asymmetric-energy e^+e^- storage ring operating at the SLAC National Accelerator Laboratory. We analyze the complete *BABAR* data sample collected at the $\Upsilon(4S)$ resonance corresponding to an integrated luminosity of 429 fb^{-1} , giving $N_{B\bar{B}} = (470.9 \pm 0.1 \pm 2.8) \times 10^6 B\bar{B}$ pairs produced, where the first uncertainty is statistical and the second systematic.

The *BABAR* detector is described in detail elsewhere [13]. Charged particles are detected and their momenta measured with a five-layer silicon vertex tracker and a 40-layer drift chamber in a 1.5 T axial magnetic

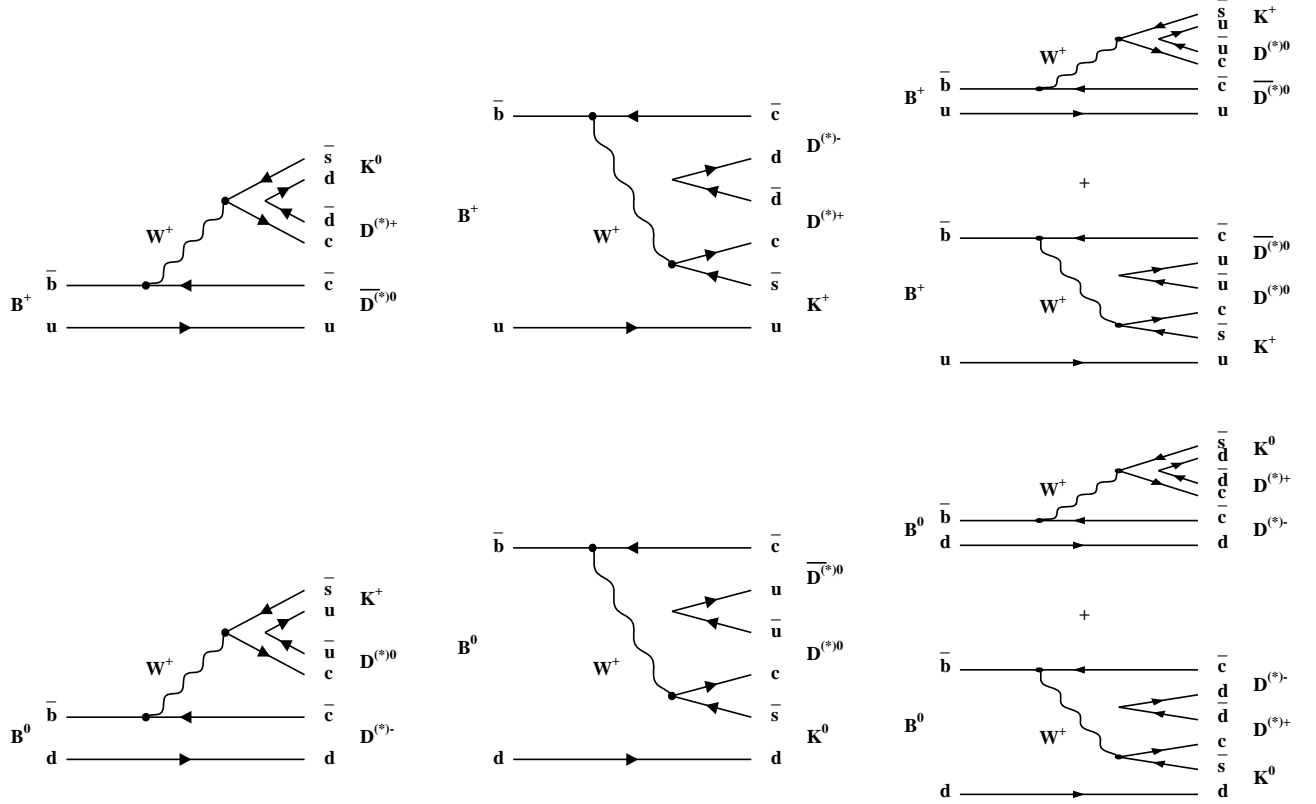


FIG. 1: Top left: external W -emission amplitude for the decays $B^+ \rightarrow \bar{D}^{(*)0} D^{(*)+} K^0$. Top center: internal W -emission amplitude for the decays $B^+ \rightarrow D^{(*)-} D^{(*)+} K^+$. Top right: external+internal W -emission amplitudes for the decays $B^+ \rightarrow \bar{D}^{(*)0} D^{(*)0} K^+$. Bottom row: same as top row respectively for $B^0 \rightarrow D^{(*)-} D^{(*)0} K^+$, $B^0 \rightarrow \bar{D}^{(*)0} D^{(*)0} K^0$ and $B^0 \rightarrow D^{(*)-} D^{(*)+} K^0$.

field. Charged particle identification is based on the measurements of the energy loss in the tracking devices and of the Cherenkov radiation in the ring-imaging detector. The energies and locations of showers associated with photons are measured in the electromagnetic calorimeter. Muons are identified by the instrumented magnetic-flux return, which is located outside the magnet.

We employ a Monte Carlo (MC) simulation to study the relevant backgrounds and estimate the selection efficiencies. We use EVTGEN [14] to model the kinematics of B mesons and JETSET [15] to model continuum processes, $e^+e^- \rightarrow q\bar{q}$ ($q = u, d, s, c$). The *BABAR* detector and its response to particle interactions are modeled using the GEANT4 [16] simulation package.

III. B CANDIDATE SELECTION

We reconstruct the B^0 and B^+ mesons in the $22 \bar{D}^{(*)} D^{(*)} K$ modes. The level of background widely varies among the signal channels, even within a specific B mode depending on the D meson decay type. A different optimization of the selection criteria is implemented for each

of the final states. The optimization determines the selection which maximizes $S/\sqrt{S+B}$, where S and B are the expected number of events for the signal and for the background in the signal region, based respectively on signal and background MC simulated events. The branching fractions for the computation of S are taken from our previous measurements of these channels [4].

We identify charged kaons using either loose or tight criteria depending on the decay mode. The loose criterion is typically 98% efficient with pion misidentification rates at the 15% level, while the tight criterion is 85% efficient with a misidentification around 2%. We use only the K_s^0 meson when a neutral K meson is present in the final state. The K_s^0 candidates are reconstructed from two oppositely charged tracks assumed to be pions consistent with coming from a common vertex and having an invariant mass within $\pm 9.5 \text{ MeV}/c^2$ of the nominal K_s^0 mass [17]. The displacement of the K_s^0 vertex in the plane transverse to the beam axis is required to be at least 0.2 cm.

The π^0 candidates are reconstructed from pairs of photons with energies $E_\gamma > 30 \text{ MeV}$ in the laboratory frame that have an invariant mass of $115 < m_{\gamma\gamma} < 150 \text{ MeV}/c^2$.

We reconstruct D mesons in the modes $D^0 \rightarrow K^-\pi^+$, $K^-\pi^+\pi^0$, $K^-\pi^+\pi^-\pi^+$, and $D^+ \rightarrow K^-\pi^+\pi^+$. The K and π tracks are required to originate from a common vertex. The invariant masses of the D candidates are required to lie within $\pm 2.5\sigma_D$ of the measured D mass, where σ_D is the D invariant mass resolution. This resolution is measured to be 5.8 MeV/ c^2 for $D^0 \rightarrow K^-\pi^+$, 9.5 MeV/ c^2 for $D^0 \rightarrow K^-\pi^+\pi^0$, 4.7 MeV/ c^2 for $D^0 \rightarrow K^-\pi^+\pi^-\pi^+$, and 4.2 MeV/ c^2 for $D^+ \rightarrow K^-\pi^+\pi^+$. To reduce the combinatorial background, for some of the B decays involving $D^0 \rightarrow K^-\pi^+\pi^0$, we use the distribution of events in the Dalitz plot of the squared invariant masses $m^2(K^-\pi^+) \times m^2(K^-\pi^0)$ where we select events that are located in the enhanced regions dominated by the $K^*(892)^+$, $K^*(892)^0$, and $\rho(770)^+$ resonances [18].

The D^* candidates are reconstructed in the decay modes $D^{*+} \rightarrow D^0\pi^+$, $D^{*+} \rightarrow D^+\pi^0$, $D^{*0} \rightarrow D^0\pi^0$, and $D^{*0} \rightarrow D^0\gamma$. The π^0 and the π^+ candidates must have a momentum smaller than 450 MeV/ c in the $\Upsilon(4S)$ rest frame, while the γ energy in the laboratory frame must be larger than 100 MeV. The mass difference between the D^{*+} and D candidates is required to be within ± 3 MeV/ c^2 of the nominal value [17]. For D^{*0} meson decays, the mass difference between the D^{*0} and D^0 candidates is required to lie between 138 and 146 MeV/ c^2 for $D^{*0} \rightarrow D^0\pi^0$ and between 130 and 150 MeV/ c^2 for $D^{*0} \rightarrow D^0\gamma$.

The B candidates are reconstructed by combining a $\bar{D}^{(*)}$, a $D^{(*)}$ and a K candidate in one of the 22 modes. For modes involving two D^0 mesons, at least one of them is required to decay to $K^-\pi^+$, except for the decay modes $D^{*-}D^{*+}K^0$, $D^{*-}D^{*+}K^+$, and $D^{*-}D^0K^+$, which have lower background and for which all combinations are accepted. For modes containing a D^{*+} meson, we look only to the decay $D^{*+} \rightarrow D^0\pi^+$, except for the modes containing $D^{*-}D^{*+}$, where we also reconstruct $D^{*+} \rightarrow D^+\pi^0$. A mass-constrained kinematic fit is applied to the intermediate particles (D^{*0} , D^{*+} , D^0 , D^+ , K_s^0 , π^0) to improve their momentum resolution.

To suppress the continuum background, we remove events with $R_2 > 0.3$ (where R_2 is the ratio of the second to zeroth Fox-Wolfram moments of the event [19]), and events with $|\cos(\theta_B)| > 0.9$ (where θ_B is the angle between the thrust axis of the candidate decay and the thrust axis of the rest of the event).

Two kinematic variables are used to isolate the B -meson signal. The first variable is the beam-energy-substituted mass defined as:

$$m_{\text{ES}} = \sqrt{\left(\frac{s/2 + \vec{p}_0 \cdot \vec{p}_B}{E_0}\right)^2 - |\vec{p}_B|^2}, \quad (1)$$

where \sqrt{s} is the e^+e^- center-of-mass energy. For the momenta \vec{p}_0 , \vec{p}_B and the energy E_0 , the subscripts 0 and B refer to the e^+e^- system and the reconstructed B meson, respectively. The other variable is ΔE , the difference between the reconstructed energy of the B candidate and the beam energy in the e^+e^- center-of-mass frame. Signal events have m_{ES} compatible with the known B -meson

mass [17] and ΔE compatible with 0 MeV, within their respective resolutions. At this stage, we keep only events which satisfy $m_{\text{ES}} > 5.20$ GeV/ c^2 .

We obtain a few signal B candidates per event on average. When the final state contains no D^* meson, we get 1.0 to 1.3 candidates per event depending on the specific mode, 1.3 to 1.9 candidates per event for final states containing one D^* meson, and 1.7 to 2.1 candidates per event when the final state contains two D^* mesons (except for $B^+ \rightarrow \bar{D}^{*0}D^{*0}K^+$ with 2.9 candidates per event). If more than one candidate is selected in an event, we retain the one with the smallest value of $|\Delta E|$ (“best candidate selection”). According to MC studies, this criterion finds the correct candidate when this one is present in the candidate list in more than 95% of the cases for final states with no D^{*0} meson and more than 80% of the cases for modes with one or two neutral D^* mesons. We keep only events with $|\Delta E| < E_c$ with E_c varying from 7 MeV to 56 MeV depending on the decay mode of the B and D mesons. The resolution on ΔE varies between 5.6 and 14.3 MeV for modes with zero or one D^{*0} meson in the final state, and between 11.6 and 19.5 MeV for modes containing two neutral D^* mesons.

The efficiency for signal events varies from 0.5% to 22.2% depending on the final state (being typically in the 5–10% range). The modes with the lowest efficiency are the ones containing one or two charged D^* mesons.

Figure 2 presents the ΔE and m_{ES} distributions after the complete selection is applied. The ΔE distributions are presented for events in the signal region defined by $m_{\text{ES}} > 5.27$ GeV/ c^2 and are shown without applying the best candidate selection. Signal events appear in the peak near $\Delta E \sim 0$ MeV when reconstructed correctly, while the peak around -160 MeV is due to \bar{D}^*DK and $\bar{D}D^*K$ decays reconstructed as $\bar{D}DK$, and to \bar{D}^*D^*K decays reconstructed as \bar{D}^*DK or $\bar{D}D^*K$. Both ΔE and m_{ES} distributions show a clear excess of events in the signal region.

IV. FITS OF THE DATA DISTRIBUTIONS

We present the fits used to extract the branching fractions. For each mode, we fit the m_{ES} distribution between 5.22 and 5.30 GeV/ c^2 to get the signal yield. The data samples corresponding to each B decay mode are disjoint and the fits are performed independently for each mode. According to their physical origin, four categories of events with differently shaped m_{ES} distributions are separately considered: $\bar{D}^{(*)}D^{(*)}K$ signal events, cross-feed events, combinatorial background events, and peaking background events. The total probability density function (PDF) is a sum of these contributions. Event yields are obtained from extended maximum likelihood unbinned fits.

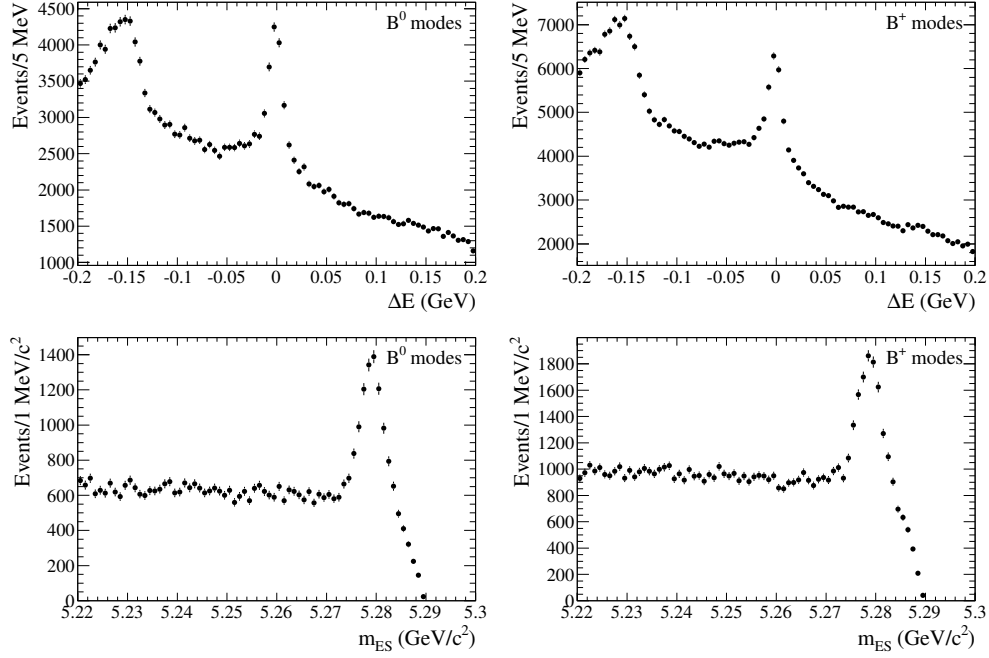


FIG. 2: Distributions of the ΔE variable (top plots) and of the m_{ES} variable (bottom plots) for the sum of all the $B^0 \rightarrow \bar{D}^{(*)} D^{(*)} K$ modes (left-hand plots) and for the sum of all the $B^+ \rightarrow \bar{D}^{(*)} D^{(*)} K$ modes (right-hand plots). The ΔE distributions are shown after the complete selection but before the choice of the best candidate and for $5.27 < m_{\text{ES}} < 5.29 \text{ GeV}/c^2$, and the m_{ES} distributions are shown after the complete selection, including the selection on the ΔE variable.

A. Signal contribution

The shape of the signal is determined from fits to the m_{ES} distributions of signal MC samples. A Crystal Ball function [20] (Gaussian modified to include a power-law tail on the low side of the peak), $\mathcal{P}_{\text{S}}(m_{\text{ES}}; m_{\text{S}}, \sigma_{\text{S}}, \alpha_{\text{S}}, n_{\text{S}})$, is used to describe the signal (see Eq. (A1) in the appendix). The parameters of this PDF are m_{S} and σ_{S} , the mean and the width of the Gaussian part, and α_{S} and n_{S} , the parameters of the tail part. The signal yield, N_{S} , is determined from the fit to the data.

B. Cross-feed contribution

We call “cross-feed” the events from all of the $\bar{D}^{(*)} D^{(*)} K$ modes, except the one we reconstruct, that pass the complete selection and that are reconstructed in the given mode. The cross-feed events are a non-negligible part of the m_{ES} peak in some of the modes, and the signal event yield must be corrected for these cross-feed events.

We observe from the analysis of simulated samples that most of the cross-feed originates from the combination of an unrelated soft π^0 or γ with the D^0 decayed from the D^{*+} to form a wrong D^{*0} candidate. The cross-feed proportion is often in the 10% range relative to the signal yield but can be comparable or larger than the signal contribution, especially for modes containing $\bar{D}^{(*)0} D^{*0}$

in the final state. To account for the cross-feed events, an iterative procedure, described in section IV F, is used to extract the signal yields and the branching fractions.

Cross-feed distributions for modes containing no D^{*0} meson can be described by a Gaussian function $\mathcal{P}_{\text{CF}}^{\text{peaking}}(m_{\text{ES}}; m_{\text{CF}}, \sigma_{\text{CF}})$ for the peaking part where m_{CF} and σ_{CF} are the mean and the width of the peaking component (Eq. (A2)). For modes containing at least one neutral D^* meson, the peaking component is described by a function $\mathcal{P}'_{\text{CF}}{}^{\text{peaking}}(m_{\text{ES}}; m_{\text{CF}}, \sigma_{\text{CF}}, t_{\text{CF}})$ which is able to model the tail at low mass (Eq. (A3)). The parameters m_{CF} and σ_{CF} represent the position of the maximum value and the width of the peak, and t_{CF} represents the tail of the function. The non-peaking part of the cross-feed contribution is described by an Argus function [21] $\mathcal{P}_{\text{CF}}^{\text{non peaking}}(m_{\text{ES}}; m_0, \xi_{\text{CF}})$ where m_0 represents the kinematic upper limit for the constrained mass and ξ_{CF} is the Argus shape parameter (Eq. (A4)).

The total PDF for cross-feed events is:

$$\mathcal{P}_{\text{CF}}(m_{\text{ES}}; m_{\text{CF}}, \sigma_{\text{CF}}, t_{\text{CF}}, m_0, \xi_{\text{CF}}) = N_{\text{CF}}^{\text{peaking}} \times \mathcal{P}_{\text{CF}}^{(\prime)\text{peaking}} + N_{\text{CF}}^{\text{non peaking}} \times \mathcal{P}_{\text{CF}}^{\text{non peaking}}, \quad (2)$$

where $\mathcal{P}_{\text{CF}}^{(\prime)\text{peaking}}$ represents either $\mathcal{P}_{\text{CF}}^{\text{peaking}}$ or $\mathcal{P}'_{\text{CF}}{}^{\text{peaking}}$ depending on the number of neutral D^* meson in the final state. The quantities $N_{\text{CF}}^{\text{peaking}}$ and $N_{\text{CF}}^{\text{non peaking}}$ are the numbers of events in the peaking PDF and in the non-peaking PDF, respectively. The values of the parameters

of the cross-feed PDF are determined by fitting signal MC m_{ES} distributions, except for the value of m_0 which is fixed to $5.2892 \text{ GeV}/c^2$. The cross-feed yield, $N_{\text{CF}} = N_{\text{CF}}^{\text{non peaking}} + N_{\text{CF}}^{\text{peaking}}$, is also extracted from the fit.

C. Combinatorial background contribution

The combinatorial background events are composed of generic B decays and of continuum events, which account respectively for about 88% and 12% of the total number of background events. The combinatorial background events are described by an Argus function $\mathcal{P}_{\text{CB}}(m_{\text{ES}}; m_0, \xi_{\text{CB}})$ where ξ_{CB} is the shape parameter (Eq. (A5)). The parameter ξ_{CB} is free to float in the fit to the data while m_0 is fixed to $5.2892 \text{ GeV}/c^2$. The yield for the combinatorial background, N_{CB} , is also obtained from the data fit.

D. Peaking background contribution

We call “peaking background” the part of the background that is peaking in the signal region and that is not due to cross-feed. To extract the peaking background, we fit the m_{ES} distributions from generic MC samples $e^+e^- \rightarrow q\bar{q}$ ($q = u, d, s, c, b$) satisfying the $\bar{D}^{(*)}D^{(*)}K$ selection and scale the results to the data luminosity.

The simulated distribution is fitted with an Argus function describing the non-peaking part and a Gaussian function $\mathcal{P}_{\text{PB}}(m_{\text{ES}}; m_{\text{PB}}, \sigma_{\text{PB}})$ describing the peaking part where m_{PB} and σ_{PB} are the mean and width of the Gaussian (Eq. (A6)). The parameters m_{PB} and σ_{PB} are free to float in the fits to the simulated events, except for modes with non-converging fits, where m_{PB} is fixed to the B mass. These modes are: $B^0 \rightarrow D^- D^+ K^0$, $B^+ \rightarrow \bar{D}^0 D^+ K^0$, $B^0 \rightarrow D^{*-} D^0 K^+$, $B^+ \rightarrow \bar{D}^{*0} D^+ K^0$, $B^+ \rightarrow \bar{D}^0 D^{*+} K^0$, $B^0 \rightarrow D^{*-} D^{*0} K^+$, $B^0 \rightarrow \bar{D}^{*0} D^{*0} K^0$, and $B^+ \rightarrow \bar{D}^{*0} D^{*0} K^+$. The fit also returns the value of the peaking background yield, N_{PB} , which is shown in Table III. Only the peaking part \mathcal{P}_{PB} is used in the fit to the data, the non-peaking part being included in the combinatorial background.

E. Fits

We fit the m_{ES} distribution using the PDFs for the signal, for the cross-feed, for the combinatorial background, and for the peaking background as detailed in the previous sections. The total PDF \mathcal{P}_{tot} can be written as:

$$\begin{aligned} \mathcal{P}_{\text{tot}} = & N_{\text{S}} \times \mathcal{P}_{\text{S}}(m_{\text{ES}}; m_{\text{S}}, \sigma_{\text{S}}, \alpha_{\text{S}}, n_{\text{S}}) \\ & + N_{\text{CF}} \times \mathcal{P}_{\text{CF}}(m_{\text{ES}}; m_{\text{CF}}, \sigma_{\text{CF}}, t_{\text{CF}}, m_0, \xi_{\text{CF}}) \\ & + N_{\text{CB}} \times \mathcal{P}_{\text{CB}}(m_{\text{ES}}; m_0, \xi_{\text{CB}}) \\ & + N_{\text{PB}} \times \mathcal{P}_{\text{PB}}(m_{\text{ES}}; m_{\text{PB}}, \sigma_{\text{PB}}). \end{aligned} \quad (3)$$

The free parameters of the fit are N_{S} , m_{S} , N_{CB} , and ξ_{CB} . All other parameters, except m_0 , are fixed to the values obtained from the simulation. For modes with low signal statistics in the data, namely $B^0 \rightarrow \bar{D}^0 D^0 K^0$, $B^0 \rightarrow \bar{D}^0 D^{*0} K^0 + \bar{D}^{*0} D^0 K^0$ and $B^0 \rightarrow \bar{D}^{*0} D^{*0} K^0$, we fix m_{S} to the value obtained from the simulation.

The free parameters are extracted by maximizing the unbinned extended likelihood

$$\mathcal{L} = \frac{e^{-N} N^n}{n!} \prod_{i=1}^n \mathcal{P}_{\text{tot}}, \quad (4)$$

where n is the number of events in the sample and N is the expectation value for the total number of events.

F. Iterative procedure

Due to the presence of cross-feed events, the fit for the branching fraction for one channel uses as inputs the branching fractions from other channels. Since these branching fractions are in principle not known, we employ an iterative procedure. In practice, we perform the complete analysis for each B mode, using as a starting point the branching fractions measured by *BABAR* in Ref. [4]. We obtain new measurements of the branching fractions that we use in the next step to fix the cross-feed proportion. We repeat this procedure until the differences between the actual branching fractions and the previous ones are smaller than 2% of the statistical uncertainty. Using this criterion, four iterations are needed. We keep the last iteration as the final result.

G. Fit results

The results of the fits are shown in Figs. 3 and 4, and are displayed in Table III. All the fits show a good description of the data. Although we perform an unbinned fit, we can compute a χ^2 value using bins of $2.5 \text{ MeV}/c^2$ width. We observe values of χ^2/N_{dof} typically close to 1, with $N_{\text{dof}} = N_{\text{bin}} - N_{\text{float}}$, where N_{bin} is the number of bins and N_{float} is the number of floating parameters in the fit.

V. BRANCHING FRACTION MEASUREMENTS

A. Method

In this paper, we measure the branching fractions of the 22 $\bar{D}^{(*)}D^{(*)}K$ modes, including non-resonant and resonant modes. It has been shown that $\bar{D}^{(*)}D^{(*)}K$ events contain resonant contributions. This was first reported by the *BABAR* Collaboration in Ref. [4] where it was observed that the three-body phase-space decay model does not give a satisfactory description of these

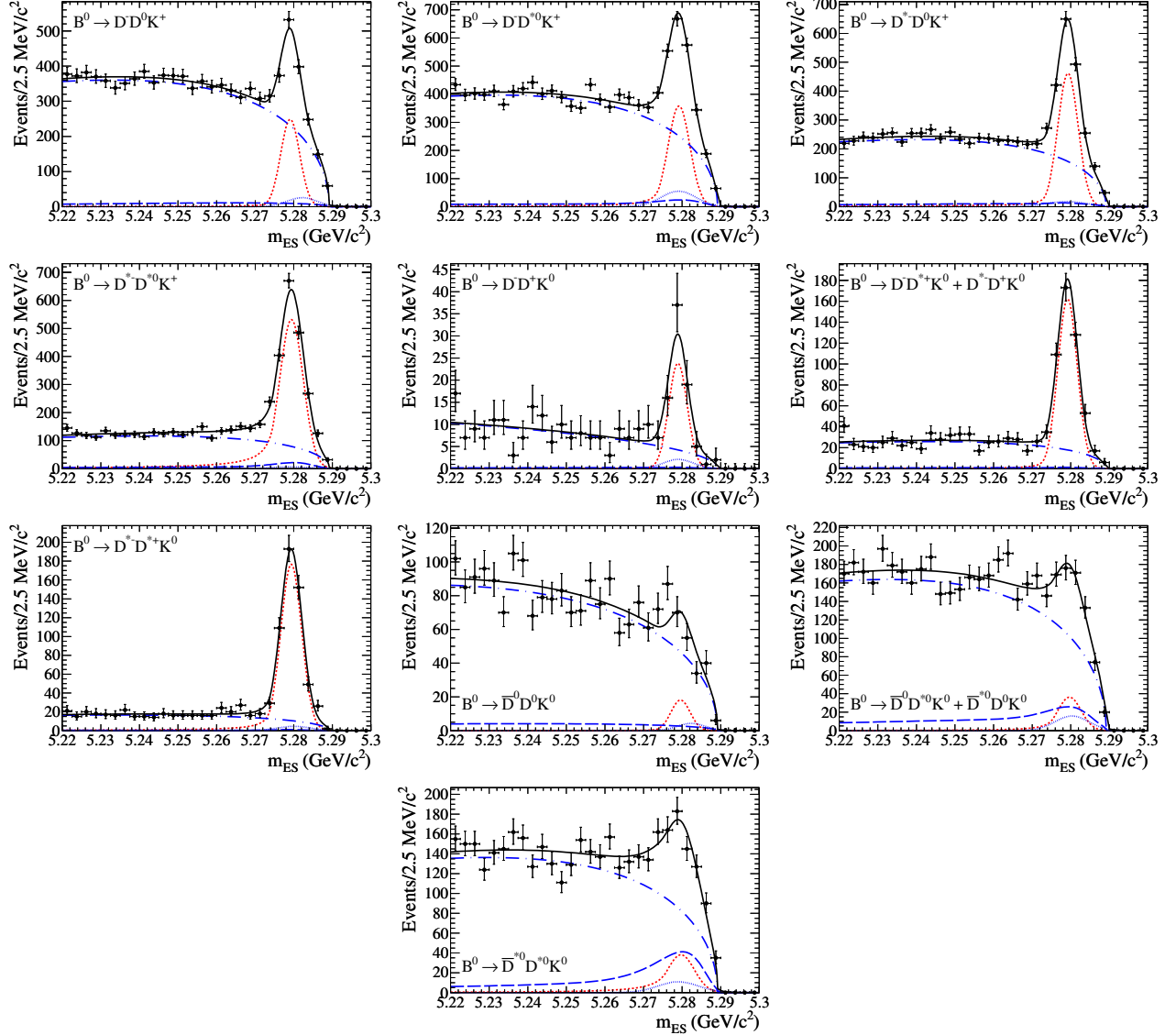


FIG. 3: Fits of the m_{ES} data distributions for the neutral modes, $B^0 \rightarrow \bar{D}^{(*)} D^{(*)} K$. The decay mode is indicated in the plots. Points with statistical errors are data events, the red dashed line represents the signal PDF, the blue long-dashed line represents the cross-feed event PDF, the blue dashed-dotted line represents the combinatorial background PDF, and the blue dotted line represents the peaking background PDF. The black solid line shows the total PDF.

decays. In a subsequent study [11], we showed the presence of $D_{s1}^+(2536)$, $\psi(3770)$ and $X(3872)$ mesons in these final states. From Belle [10], we know that the $D_{sJ}(2700)$ meson has a large contribution in the mode $B^+ \rightarrow \bar{D}^0 D^0 K^+$. This meson is expected to be present in $\bar{D}^{(*)} D^{(*)} K$ final states containing $D^0 K^+$ and $D^+ K^0$, as well as in the final states containing $D^{*0} K^+$ and $D^{*+} K^0$, since it was recently seen decaying to $D^* K$ [22]. There is in addition the possibility of having unknown resonances in the $\bar{D}^{(*)} D^{(*)} K$ final states. Simulations of the known resonances indicate that the efficiencies for non-resonant modes and resonant modes are significantly different. This is due to the fact that the efficiency is not uniform

across the phase space and that resonant events, depending on the mass, the width and the spin of the resonance, populate differently the Dalitz plane. Ignoring this effect would introduce a bias of up to 9% in the total branching fraction for some decay modes. In order to measure the branching fractions inclusively without any assumptions on the resonance structure of the signal, we estimate the efficiency as a function of location in the Dalitz plane of the squared invariant masses $m^2(\bar{D}^{(*)} D^{(*)}) \times m^2(D^{(*)} K)$ for the data. We use this efficiency at the event position in the Dalitz plane to reweight the signal contribution. To isolate the signal contribution event-per-event, we use the `sPlot` technique [23].

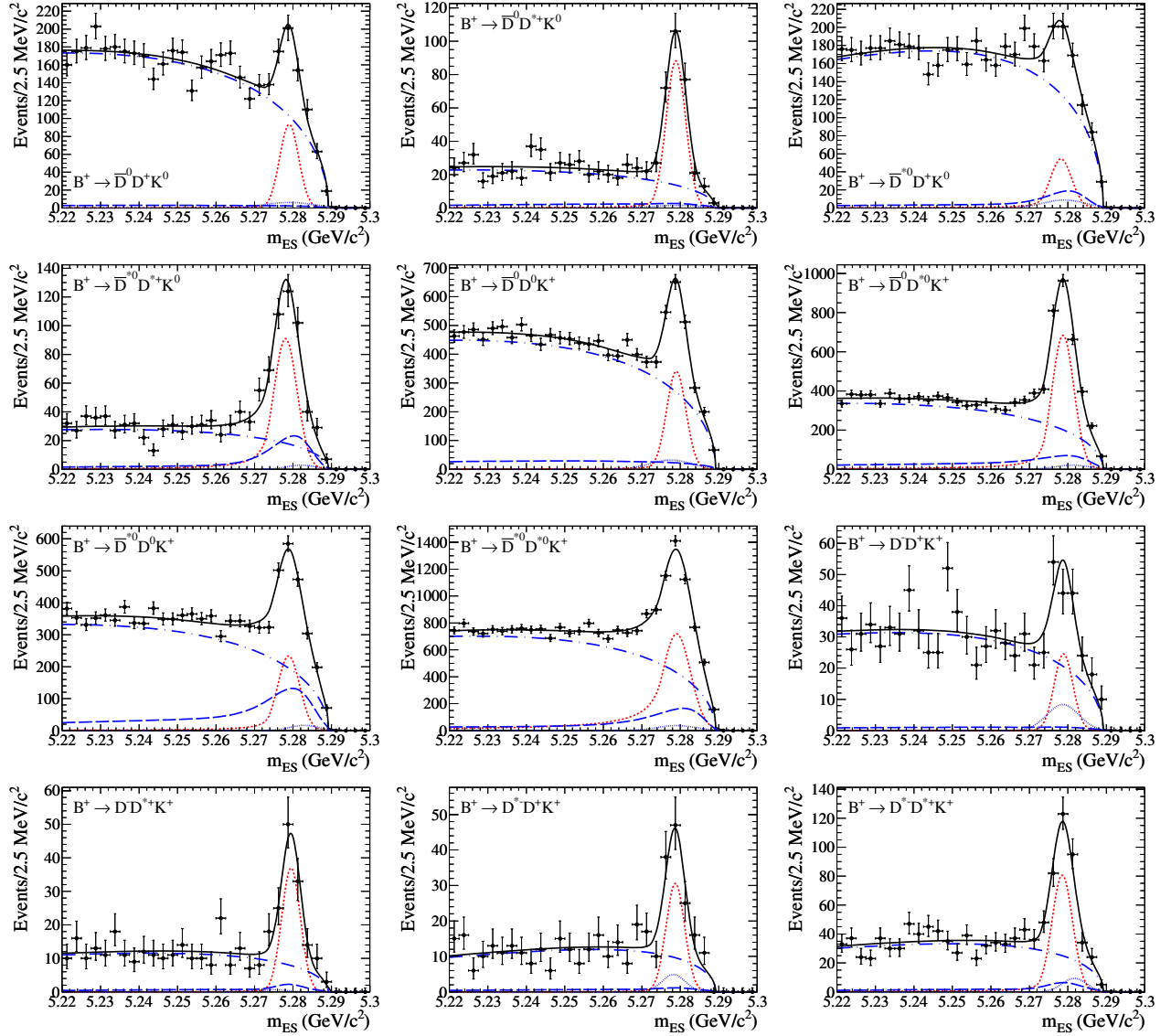


FIG. 4: Fits of the m_{ES} data distributions for the charged modes, $B^+ \rightarrow \bar{D}^{(*)} D^{(*)} K$. The decay mode is indicated in the plots. Points with statistical errors are data events, the red dashed line represents the signal PDF, the blue long-dashed line represents the cross-feed event PDF, the blue dashed-dotted line represents the combinatorial background PDF, and the blue dotted line represents the peaking background PDF. The black solid line shows the total PDF.

The `sPlot` technique exploits the result of the m_{ES} fit (yield and covariance matrix) and the PDFs of this fit to compute an event-per-event weight for the signal category and background category. The PDF for the signal category is \mathcal{P}_S . For the background category, the three PDFs for the different components of the background (cross-feed, combinatorial events, and peaking background) are combined together to form one PDF:

$$\mathcal{P}_B = \frac{N_{CF} \times \mathcal{P}_{CF} + N_{CB} \times \mathcal{P}_{CB} + N_{PB} \times \mathcal{P}_{PB}}{N_B}, \quad (5)$$

where N_B is the sum of the background yields, $N_B = N_{CF} + N_{CB} + N_{PB}$. The PDFs and the yields are the ones obtained from the results in section IV.

The `sPlot` weight for the signal category is defined as:

$$w_S(i) = \frac{V_{S,S} \mathcal{P}_S(i) + V_{S,B} \mathcal{P}_B(i)}{N_S \mathcal{P}_S(i) + N_B \mathcal{P}_B(i)}. \quad (6)$$

Here, i stands for the index of the event, with $\mathcal{P}_j(i)$ ($j = S, B$) corresponding to the value of the PDF for the event i . The quantity $V_{S,j}$ ($j = S, B$) is the covariance matrix element between the signal yield N_S and the yield N_j .

The branching fraction for a specific $\bar{D}^{(*)} D^{(*)} K$ mode is given by:

$$\mathcal{B} = \sum_i \frac{w_S(i)}{N_{B\bar{B}} \times \langle \varepsilon_{B_{sub}} \rangle_i}, \quad (7)$$

where we define:

$$\langle \varepsilon \mathcal{B}_{\text{sub}} \rangle_i = \sum_j \varepsilon_{ij} \times \mathcal{B}_{\text{sub},j}. \quad (8)$$

The sum on j is over all the D subdecays of a particular $\bar{D}^{(*)}D^{(*)}K$ mode. The term $\mathcal{B}_{\text{sub},j}$ is the product of the secondary branching fractions of the subdecay j :

$$\mathcal{B}_{\text{sub},j} = \mathcal{B}_{\bar{D}^{(*)}} \times \mathcal{B}_{D^{(*)}} \times \mathcal{B}_K, \quad (9)$$

where $\mathcal{B}_{\bar{D}^{(*)}}$, $\mathcal{B}_{D^{(*)}}$, and \mathcal{B}_K are the secondary branching fractions of the $\bar{D}^{(*)}$, $D^{(*)}$ and K mesons [17] (with $\mathcal{B}_K = 1$ for K^+ mesons). The quantity ε_{ij} is the efficiency for the subdecay j at the Dalitz position of event i . In practice, for a specific $\bar{D}^{(*)}D^{(*)}K$ mode with given D subdecays (e.g. $\bar{D}^0 \rightarrow K^+\pi^- \times D^0 \rightarrow K^-\pi^+\pi^0$), the efficiency is obtained by using the specific simulated signal and dividing the reconstructed signal by the generated signal in the Dalitz plane $m^2(\bar{D}^{(*)}D^{(*)}) \times m^2(D^{(*)}K)$, which is divided in 15×15 bins for the operation. The size of the bins is roughly $0.52 \times 0.77 \text{ GeV}^2/c^4$, $0.46 \times 0.68 \text{ GeV}^2/c^4$, and $0.38 \times 0.58 \text{ GeV}^2/c^4$ for decay modes with no D^* , one D^* and two D^* mesons respectively, depending on the available phase space. Neighboring bins are added together if one bin contains fewer than 10 events in the reconstructed Dalitz plane. The signal is simulated assuming a flat (phase space) distribution in this Dalitz plane.

The statistical uncertainty on the branching fraction is given by [23]:

$$\sigma_B = \sqrt{\sum_i \left(\frac{w_S(i)}{N_{B\bar{B}} \times \langle \varepsilon \mathcal{B}_{\text{sub}} \rangle_i} \right)^2}. \quad (10)$$

B. Validation

The analysis is validated at all stages by use of MC samples. These samples consist of a mixture of continuum events and generic B decays containing the $\bar{D}^{(*)}D^{(*)}K$ signals with branching fractions close to the ones measured in our previous result [4]. As a preliminary remark, it has to be noted that the analysis technique, including the selection optimization and the procedure for the fit and for the branching fraction measurement, is first determined solely on MC simulations (“blind” analysis).

First, we show that the fit is able to find the true number of simulated signal events within a 1σ interval for the 22 modes, where σ is the statistical uncertainty reported by the fit.

Furthermore, the **sPlot** method is tested on simulated samples. It is shown that this technique is able to tag true MC signal events with very good performance. A feature of the **sPlot** method is that the sum of **sPlot** weights for a given category is equal to the yield of this category [23]. We determine that the sum of **sPlot** signal weights for the MC signal events is equal to the number

of simulated MC signal events with a relative difference smaller than 1.5% for the majority of the modes. We also check that the sum of **sPlot** signal weights for the MC background events is compatible with zero as expected.

Finally, we perform the measurement on MC simulations and find that the analysis is able to find the branching fractions set in the simulation within a 1σ interval for most of the 22 modes, where σ is the total uncertainty on the branching fraction (combining in quadrature statistical and systematic uncertainties). We also test the iterative procedure by randomizing the initial branching fractions and check that the branching fractions are converging to the expected values after a few iterations.

C. Measurement

For each event, we obtain the **sPlot** weight as well as the efficiency at its Dalitz position. Using Eq. (7) we compute the branching fraction for each of the B modes. We present these results in Table III. We assume equal $B^0\bar{B}^0$ and B^+B^- production [17].

VI. SYSTEMATIC UNCERTAINTIES

We consider several sources of systematic uncertainties on the branching fraction measurements. Their contributions are summarized in Table II.

(a) We fix the width of the signal PDF from the value obtained in the fit to the signal MC sample. To estimate the systematic uncertainties originating from this choice, we repeat the fit with the width free to float for modes with high significance, namely $B^0 \rightarrow D^-D^{*+}K^0 + D^{*-}D^+K^0$, $B^0 \rightarrow D^{*-}D^{*+}K^0$, $B^0 \rightarrow D^{*-}D^{*0}K^+$ and $B^+ \rightarrow \bar{D}^0D^{*+}K^0$. The difference observed between the width from the data and from the MC events is roughly equal to $0.1 \text{ MeV}/c^2$. Using this number, we repeat the fits for all modes adding $\pm 0.1 \text{ MeV}/c^2$ to the value of the width. The difference with the nominal branching fraction gives the systematic contribution associated to the signal shape. In addition, as mentioned in section IV E, three $\bar{D}^{(*)}D^{(*)}K$ modes with low signal statistics have their PDF mean fixed to the value obtained for the simulation. We repeat the fit using the PDF mean obtained from a mode with a large statistics (namely $B^0 \rightarrow D^{*-}D^{*+}K^0$) and take the difference in branching fraction as the systematic uncertainty. These two contributions of the systematic uncertainties are added in quadrature.

(b) The cross-feed determination introduces systematic uncertainties of which two sources are identified. First, we use an alternate function for the cross-feed PDF (using a non-parametric function rather than Eq. (2)), which gives relative systematic uncertainties below 1%. Second, the cross-feed branching fractions and their uncertainties are known from the results of this analysis. To estimate the systematic uncertainties coming from this effect, we

TABLE II: Summary of the absolute systematic uncertainties on the branching fractions for each $\bar{D}^{(*)}D^{(*)}K$ mode (in units of 10^{-4}). The values listed in this table correspond to the systematic uncertainties associated with the signal shape (a), the cross-feed contribution (b), the peaking background (c), the combinatorial background (d), the fit bias (e), the iterative procedure (f), the limited MC statistics (g), the number of bins of the Dalitz plane (h), the particle detection efficiency (i) and finally the secondary branching fractions and the number of $B\bar{B}$ pairs (j). The letters in parenthesis refer to the specific paragraph in section VI. The last column presents the total systematic uncertainties.

Mode	Signal shape (a)	Cross- feed (b)	Peaking back. (c)	Comb. back. (d)	Fit bias (e)	Iter. proc. (f)	MC stat. (g)	Bins (h)	Particle detection (i)	BF + $N_{B\bar{B}}$ (j)	Total syst.
B^0 decays through external W -emission amplitudes											
$B^0 \rightarrow D^- D^0 K^+$	0.2	0.1	0.5	0.0	0.0	0.0	0.2	0.2	0.5	0.3	0.9
$B^0 \rightarrow D^- D^{*0} K^+$	0.7	0.1	2.4	0.0	0.0	0.1	1.3	1.1	1.9	1.1	3.7
$B^0 \rightarrow D^{*-} D^0 K^+$	0.5	0.0	0.7	0.0	0.0	0.0	0.5	0.5	1.3	0.8	1.8
$B^0 \rightarrow D^{*-} D^{*0} K^+$	2.0	0.2	1.6	0.1	0.0	0.2	1.8	3.8	6.4	2.9	8.6
B^0 decays through external+internal W -emission amplitudes											
$B^0 \rightarrow D^- D^+ K^0$	0.1	0.0	1.0	0.0	0.2	0.0	0.1	0.1	0.2	0.4	1.2
$B^0 \rightarrow D^- D^{*+} K^0 + D^{*-} D^+ K^0$	0.9	0.0	1.3	0.1	0.1	0.0	1.3	0.9	2.4	2.2	3.9
$B^0 \rightarrow D^{*-} D^{*+} K^0$	1.2	0.0	2.0	0.0	0.0	0.0	3.2	2.1	4.2	2.9	6.7
B^0 decays through internal W -emission amplitudes											
$B^0 \rightarrow \bar{D}^0 D^0 K^0$	0.2	0.0	0.4	0.1	0.1	0.0	0.1	0.2	0.1	0.1	0.5
$B^0 \rightarrow \bar{D}^0 D^{*0} K^0 + \bar{D}^{*0} D^0 K^0$	0.3	0.4	3.4	0.1	0.5	0.1	0.5	0.3	0.5	0.3	3.6
$B^0 \rightarrow \bar{D}^{*0} D^{*0} K^0$	0.9	1.6	5.2	0.2	0.8	1.8	1.1	2.6	1.7	0.6	6.7
B^+ decays through external W -emission amplitudes											
$B^+ \rightarrow \bar{D}^0 D^+ K^0$	0.4	0.0	0.9	0.1	0.0	0.0	0.3	0.2	0.5	0.5	1.3
$B^+ \rightarrow \bar{D}^0 D^{*+} K^0$	0.5	0.3	1.0	0.1	0.1	0.0	0.8	0.3	1.4	1.0	2.3
$B^+ \rightarrow \bar{D}^{*0} D^+ K^0$	0.5	0.3	2.5	0.3	0.3	0.3	0.8	0.5	1.0	0.7	3.0
$B^+ \rightarrow \bar{D}^{*0} D^{*+} K^0$	1.6	1.3	2.5	0.1	0.1	0.4	3.1	5.5	4.9	2.4	9.0
B^+ decays through external+internal W -emission amplitudes											
$B^+ \rightarrow \bar{D}^0 D^0 K^+$	0.3	0.0	1.0	0.0	0.0	0.0	0.2	0.2	0.6	0.3	1.2
$B^+ \rightarrow \bar{D}^0 D^{*0} K^+$	1.2	0.2	1.0	0.0	0.1	0.3	0.9	1.4	3.6	1.6	4.5
$B^+ \rightarrow \bar{D}^{*0} D^0 K^+$	0.4	0.2	0.5	0.0	0.1	0.3	0.6	0.5	1.3	0.6	1.7
$B^+ \rightarrow \bar{D}^{*0} D^{*0} K^+$	2.0	0.6	2.8	0.7	0.2	1.3	4.2	6.2	9.0	3.0	12.6
B^+ decays through internal W -emission amplitudes											
$B^+ \rightarrow D^- D^+ K^+$	0.1	0.0	0.5	0.0	0.1	0.0	0.0	0.0	0.1	0.1	0.5
$B^+ \rightarrow D^- D^{*+} K^+$	0.1	0.0	0.4	0.0	0.0	0.0	0.2	0.3	0.3	0.2	0.6
$B^+ \rightarrow D^{*-} D^+ K^+$	0.1	0.0	0.6	0.1	0.0	0.0	0.3	0.1	0.3	0.2	0.8
$B^+ \rightarrow D^{*-} D^{*+} K^+$	0.2	0.0	0.5	0.0	0.1	0.0	0.6	0.2	0.7	0.4	1.2

repeat the measurement applying $\pm 1\sigma$ of the statistical uncertainty on each cross-feed contribution to a given mode. These different contributions for each cross-feed mode are then combined quadratically.

(c) The peaking background contributions are fixed from fits to the background MC simulation, using a Gaussian PDF. In these fits, the three parameters, namely the number of events, the mean and the width, are correlated. We generate several sets of these parameters based on the covariance matrix of the fits and recompute the branching fractions for each of these sets. From the distribution of the branching fractions, we extract the systematic uncertainties originating from the peaking background. Another systematic effect arises from the fact that we use the MC after having scaled it to the data luminosity (using the total number of MC events passing the selection, the number of $B\bar{B}$ pairs and the

cross-section of $e^+e^- \rightarrow q\bar{q}$, where $q = u, d, s, c$). We estimate the data-MC agreement by computing the ratio of number of events for data and simulation for m_{ES} between 5.22 and 5.25 GeV/ c^2 . We rescale the peaking background events using the ratio found in the specific mode (0.9 in average), and repeat the branching fraction measurement. The difference with the nominal branching fraction gives the systematic uncertainty related to this effect. We combine these two sources of uncertainties in quadrature. Given the difficulty of estimating the peaking background, this is the dominant systematic uncertainty for most of the $\bar{D}^{(*)}D^{(*)}K$ modes.

(d) The systematic uncertainty associated with the assumption of a fixed value of the end point in the Argus function is estimated by repeating the fit and letting the end point free to vary in the physical region between 5.288 and 5.292 GeV/ c^2 , to account for possible varia-

tions in the beam energy measurement. The difference in the branching fraction between this fit and the nominal fit gives the systematic contribution related to the combinatorial background.

(e) We investigate the fit procedure performing a large number of test fits to MC samples obtained from the PDFs fitted to the data, and look for the presence of possible bias in the number of signal events. We observe that the biases are in most cases smaller than 10% of the statistical uncertainty. We do not correct these small biases but take them into account in the total systematic uncertainties.

(f) An iterative procedure is performed to compute the branching fractions. We check this procedure on the MC simulation where the results should not depend on the procedure used. The difference between the iterative and non-iterative methods is small but non negligible in some cases. We take the relative difference as the systematic contribution on the data due to the iterative procedure.

(g) The limited Monte Carlo statistics induce an uncertainty on the computation of the signal efficiency. We use an efficiency mapping in the Dalitz plane with 15×15 bins. To take into account this uncertainty, we generate several efficiency mappings where in each bin we vary the nominal efficiency according to the efficiency uncertainty distribution. We obtain a distribution of branching fractions that we employ to determine the systematic contribution.

(h) We extract the efficiency in the Dalitz plane from a 15×15 bin mapping. We vary the numbers of bins from 1×1 bin to 20×20 bins and recompute the branching fractions. This test is performed on MC simulation containing signal and background events, where the $\bar{D}^{(*)}D^{(*)}K$ signal is purely non-resonant. In this case, the results should not depend on the number of bins since no resonant states are present. The maximal difference with the nominal branching fraction is taken as the systematic uncertainty.

(i) From the differences in the reconstruction and particle identification efficiencies for the data and MC control samples, we derive systematic uncertainties of 0.2% per charged track, 1.7% per soft pion from D^* decays, 1.2% per K_s^0 , 3% per π^0 and 1.8% per single photon. Additionally, the systematic uncertainties for the K^+ identification are ranging from 2 to 4% (in total) depending on the mode.

(j) Finally, the uncertainties on the $D^{(*)}$ and K_s^0 branching fractions [17] are accounted for. The total systematic uncertainty also takes into account the number of B mesons in the data sample which is known with a 0.6% uncertainty.

Table II shows a summary of the systematic uncertainties. The uncertainties from the different contributions are added together in quadrature to give the total systematic uncertainty for a specific mode.

VII. RESULTS

The final results on the data using the full *BABAR* data sample can be found in Table III. In this Table, the quantity $N_{\text{CF}}^{\text{SR}}$ is the number of cross-feed events in the signal region (*i.e.* integrating the cross-feed PDF for $m_{\text{ES}} > 5.27 \text{ GeV}/c^2$) determined from the MC simulation scaled to the data luminosity using the branching fractions measured in this analysis (this includes peaking and non-peaking cross-feed contributions). We indicate the significances (including systematic uncertainties) of the observations. To compute these significances, we repeat the fits using no contribution from the signal. We compute the statistical significance S_{stat} calculating $\text{PROB}(2 \ln(\mathcal{L}_{\text{signal}}/\mathcal{L}_0), N_{\text{dof}})$, where $\mathcal{L}_{\text{signal}}$ (\mathcal{L}_0) is the maximum of the likelihood with (without) the signal contribution, N_{dof} is the number of free parameters in the signal PDF (two here) and PROB is the upper tail probability of a chi-squared distribution, converting this probability into a number of standard deviations. We then take the systematic uncertainty into account by smearing S_{stat} by use of a Gaussian with a width equal to the systematic uncertainty: $S_{\text{stat+syst}} = S_{\text{stat}}/\sqrt{(1 + \sigma_{\text{syst}}^2/\sigma_{\text{stat}}^2)}$, where σ_{stat} and σ_{syst} are respectively the statistical and systematic uncertainties on the branching fraction measurement.

We check isospin invariance using the $\bar{D}^{(*)}D^{(*)}K$ decays. Assuming isospin invariance in the B decay, interchanging the u and d quarks in the Feynman diagrams of Fig. 1 should not modify the amplitude values. Table IV presents the ratios of the modes which are related by isospin symmetry. In the ratio of the branching fractions, all factors cancel except the amplitudes and the B^0/B^+ lifetimes (neglecting the small mass differences between neutral and charged states for the B , D^* , D and K mesons). We multiply the ratios of the neutral to charged branching fractions, r , by the ratio of the charged to neutral B meson lifetimes, $\tau_{B^+}/\tau_{B^0} = 1.071 \pm 0.009$ [17]. The uncertainty on these values reported in Table IV combines the statistical and systematic uncertainties of our measurement, as well as the uncertainty on the lifetime ratio. The values of $r \times \tau_{B^+}/\tau_{B^0}$ should be equal to unity if isospin invariance is verified. Although some values are compatible with this equality, for some others we observe discrepancies up to 2.6σ (where σ is the 68% standard deviation). This result is obtained assuming equal production of B^0 and B^+ mesons.

VIII. CONCLUSION

We have analyzed 471 million pairs of B mesons produced in the *BABAR* experiment, and studied the exclusive decays of B^0/\bar{B}^0 , B^\pm to $\bar{D}^{(*)}D^{(*)}K^\pm$ and B^0/\bar{B}^0 , B^\pm to $\bar{D}^{(*)}D^{(*)}K^0$. We measure the branching fractions for the 22 modes (see Table III). Some of the modes have been observed for the first time here: $B^+ \rightarrow \bar{D}^{*0}D^0K^+$

TABLE III: Number of events for the signal, N_S , for the peaking background, N_{PB} , and for the cross-feed in the signal region, N_{CF}^{SR} , and branching fractions in units of 10^{-4} . The yields N_S and N_{PB} are defined on the whole m_{ES} range whereas N_{CF}^{SR} is defined for $m_{ES} > 5.27 \text{ GeV}/c^2$. The first uncertainties are statistical and the second are systematic. The last column presents the significances including the systematic uncertainties.

Mode	N_S	N_{PB}	N_{CF}^{SR}	\mathcal{B}	Significance
B^0 decays through external W -emission amplitudes					
$B^0 \rightarrow D^- D^0 K^+$	635 ± 47	99 ± 54	65	$10.7 \pm 0.7 \pm 0.9$	8.6σ
$B^0 \rightarrow D^- D^{*0} K^+$	1116 ± 64	250 ± 69	137	$34.6 \pm 1.8 \pm 3.7$	7.6σ
$B^0 \rightarrow D^{*-} D^0 K^+$	1300 ± 54	93 ± 40	78	$24.7 \pm 1.0 \pm 1.8$	12.6σ
$B^0 \rightarrow D^{*-} D^{*0} K^+$	1883 ± 63	31 ± 28	112	$106.0 \pm 3.3 \pm 8.6$	11.4σ
B^0 decays through external+internal W -emission amplitudes					
$B^0 \rightarrow D^- D^+ K^0$	58 ± 10	8 ± 11	2	$7.5 \pm 1.2 \pm 1.2$	5.1σ
$B^0 \rightarrow D^- D^{*+} K^0 + D^{*-} D^+ K^0$	422 ± 25	0 ± 12	7	$64.1 \pm 3.6 \pm 3.9$	13.4σ
$B^0 \rightarrow D^{*-} D^{*+} K^0$	511 ± 27	20 ± 13	5	$82.6 \pm 4.3 \pm 6.7$	12.5σ
B^0 decays through internal W -emission amplitudes					
$B^0 \rightarrow \bar{D}^0 D^0 K^0$	46 ± 19	15 ± 19	19	$2.7 \pm 1.0 \pm 0.5$	2.3σ
$B^0 \rightarrow \bar{D}^0 D^{*0} K^0 + \bar{D}^{*0} D^0 K^0$	126 ± 39	70 ± 39	147	$10.8 \pm 3.2 \pm 3.6$	2.2σ
$B^0 \rightarrow \bar{D}^{*0} D^{*0} K^0$	170 ± 49	58 ± 31	231	$24.0 \pm 5.5 \pm 6.7$	2.2σ
B^+ decays through external W -emission amplitudes					
$B^+ \rightarrow \bar{D}^0 D^+ K^0$	237 ± 30	40 ± 23	16	$15.5 \pm 1.7 \pm 1.3$	6.6σ
$B^+ \rightarrow \bar{D}^0 D^{*+} K^0$	233 ± 19	9 ± 10	17	$38.1 \pm 3.1 \pm 2.3$	10.7σ
$B^+ \rightarrow \bar{D}^{*0} D^+ K^0$	164 ± 37	48 ± 33	95	$20.6 \pm 3.8 \pm 3.0$	3.3σ
$B^+ \rightarrow \bar{D}^{*0} D^{*+} K^0$	308 ± 28	11 ± 12	113	$91.7 \pm 8.3 \pm 9.0$	7.5σ
B^+ decays through external+internal W -emission amplitudes					
$B^+ \rightarrow \bar{D}^0 D^0 K^+$	901 ± 54	173 ± 77	153	$13.1 \pm 0.7 \pm 1.2$	8.6σ
$B^+ \rightarrow \bar{D}^0 D^{*0} K^+$	2180 ± 74	92 ± 50	409	$63.2 \pm 1.9 \pm 4.5$	12.5σ
$B^+ \rightarrow \bar{D}^{*0} D^0 K^+$	745 ± 60	61 ± 26	724	$22.6 \pm 1.6 \pm 1.7$	8.3σ
$B^+ \rightarrow \bar{D}^{*0} D^{*0} K^+$	3530 ± 141	186 ± 65	928	$112.3 \pm 3.6 \pm 12.6$	6.8σ
B^+ decays through internal W -emission amplitudes					
$B^+ \rightarrow D^- D^+ K^+$	60 ± 15	35 ± 20	7	$2.2 \pm 0.5 \pm 0.5$	2.8σ
$B^+ \rightarrow D^- D^{*+} K^+$	91 ± 13	2 ± 7	10	$6.3 \pm 0.9 \pm 0.6$	6.7σ
$B^+ \rightarrow D^{*-} D^+ K^+$	75 ± 13	15 ± 9	6	$6.0 \pm 1.0 \pm 0.8$	5.1σ
$B^+ \rightarrow D^{*-} D^{*+} K^+$	232 ± 23	30 ± 14	31	$13.2 \pm 1.3 \pm 1.2$	7.4σ

(8.3σ), $B^+ \rightarrow D^{*-} D^{*+} K^+$ (7.4σ), $B^+ \rightarrow D^- D^{*+} K^+$ (6.7σ), $B^+ \rightarrow \bar{D}^0 D^+ K^0$ (6.6σ), and $B^0 \rightarrow D^- D^+ K^0$ (5.1σ). In addition, we show evidence for the mode $B^+ \rightarrow \bar{D}^{*0} D^+ K^0$ (3.3σ) for the first time. We also report the observation of some of the color-suppressed modes, namely $B^+ \rightarrow D^{*-} D^{*+} K^+$ (7.4σ), $B^+ \rightarrow D^- D^{*+} K^+$ (6.7σ), and $B^+ \rightarrow D^{*-} D^+ K^+$ (5.1σ). The other color-suppressed modes are seen with a lower significance: $B^+ \rightarrow D^- D^+ K^+$ (2.8σ), $B^0 \rightarrow \bar{D}^0 D^0 K^0$ (2.3σ), $B^0 \rightarrow \bar{D}^{*0} D^{*0} K^0$ (2.2σ), and $B^0 \rightarrow \bar{D}^0 D^{*0} K^0 + \bar{D}^{*0} D^0 K^0$ (2.2σ).

Summing the 10 neutral modes and the 12 charged modes, we measure that $\bar{D}^{(*)} D^{(*)} K$ events represent $(3.68 \pm 0.10 \pm 0.24)\%$ of the B^0 decays and $(4.05 \pm 0.11 \pm 0.28)\%$ of the B^+ decays, where the first uncertainties are statistical and the second systematic, taking into account the correlations amongst the systematic uncertainties. These decays do not saturate the wrong-sign D production, and account roughly for one third of this production. This result implies that probably decays of the type $B \rightarrow \bar{D}^{(*)} D^{(*)} K(n\pi)$ (with $n \geq 1$) have

a non-negligible contribution to the $b \rightarrow c\bar{c}s$ transition (for example through the decays $B \rightarrow \bar{D}^{(*)} D^{(*)} K^*$ or $B \rightarrow \bar{D}^{(*)} D^{**} K$ where D^{**} is an excited D meson other than D^{*+} and D^{*0}).

The results obtained here are found to be in satisfactory agreement with those of the previous study by BABAR using 76 fb^{-1} [4] and supersede these previous measurements. Our branching fraction measurement of the mode $B^0 \rightarrow D^{*-} D^{*+} K^0$ is found in good agreement with the values reported in Ref. [8] and Ref. [9], and supersedes our previous result [8]. However, our branching fraction measurement of the mode $B^+ \rightarrow \bar{D}^0 D^0 K^+$ is in disagreement at a 2.1σ level with the Belle result [10].

We believe that the discrepancy with Ref. [10] and the fact that the branching fractions measured here are almost systematically lower than the ones in Ref. [4] (although most of the time compatible) are due to the fact that in the present work we employ a more accurate parametrization of the signal m_{ES} distribution in the fit and that we take into account both the cross-feed and the peaking background contributions. In Ref. [4], only cross-

TABLE IV: Ratios of neutral to charged branching fractions. The second column shows the ratio r where the first uncertainty is statistical and the second is systematic. The third column shows this value multiplied by the ratio of the charged to neutral B meson lifetimes, where the error includes all uncertainties.

Mode	r	$r \times \tau_{B^+}/\tau_{B^0}$
$\mathcal{B}(B^0 \rightarrow D^- D^0 K^+)/\mathcal{B}(B^+ \rightarrow \bar{D}^0 D^+ K^0)$	$0.69 \pm 0.09 \pm 0.08$	0.74 ± 0.13
$\mathcal{B}(B^0 \rightarrow D^- D^{*0} K^+)/\mathcal{B}(B^+ \rightarrow \bar{D}^{*0} D^+ K^0)$	$0.91 \pm 0.09 \pm 0.11$	0.97 ± 0.15
$\mathcal{B}(B^0 \rightarrow D^{*-} D^0 K^+)/\mathcal{B}(B^+ \rightarrow \bar{D}^{*0} D^+ K^0)$	$1.20 \pm 0.23 \pm 0.20$	1.28 ± 0.32
$\mathcal{B}(B^0 \rightarrow D^{*-} D^{*0} K^+)/\mathcal{B}(B^+ \rightarrow \bar{D}^{*0} D^{*+} K^0)$	$1.16 \pm 0.11 \pm 0.15$	1.24 ± 0.20
$\mathcal{B}(B^0 \rightarrow D^- D^+ K^0)/\mathcal{B}(B^+ \rightarrow \bar{D}^0 D^0 K^+)$	$0.57 \pm 0.10 \pm 0.10$	0.61 ± 0.15
$\mathcal{B}(B^0 \rightarrow D^- D^{*+} K^0 + D^{*-} D^+ K^0)$	$0.75 \pm 0.05 \pm 0.07$	0.80 ± 0.09
$\mathcal{B}(B^+ \rightarrow \bar{D}^0 D^{*0} K^+) + \mathcal{B}(B^+ \rightarrow \bar{D}^{*0} D^0 K^+)$		
$\mathcal{B}(B^0 \rightarrow D^{*-} D^{*+} K^0)/\mathcal{B}(B^+ \rightarrow \bar{D}^{*0} D^{*0} K^+)$	$0.74 \pm 0.05 \pm 0.10$	0.79 ± 0.12
$\mathcal{B}(B^0 \rightarrow \bar{D}^0 D^0 K^0)/\mathcal{B}(B^+ \rightarrow D^- D^+ K^+)$	$1.20 \pm 0.53 \pm 0.36$	1.28 ± 0.69
$\mathcal{B}(B^0 \rightarrow \bar{D}^0 D^{*0} K^0 + \bar{D}^{*0} D^0 K^0)$		
$\mathcal{B}(B^+ \rightarrow D^- D^{*+} K^+) + \mathcal{B}(B^+ \rightarrow D^{*-} D^+ K^+)$	$0.88 \pm 0.27 \pm 0.31$	0.94 ± 0.44
$\mathcal{B}(B^0 \rightarrow \bar{D}^{*0} D^{*0} K^0)/\mathcal{B}(B^+ \rightarrow D^{*-} D^{*+} K^+)$	$1.81 \pm 0.45 \pm 0.53$	1.94 ± 0.75

feed was accounted for but the peaking background was not considered due to the lower statistics. In addition, the efficiency correction used in obtaining the branching fractions accounts for the presence of resonant intermediate states in the data.

Finally, from neutral to charged B meson ratios of the branching fractions, assuming equal $B^0 \bar{B}^0$ and $B^+ B^-$ production and taking into account the B meson lifetimes, we note that some mode ratios respect the isospin invariance while some others show discrepancies up to 2.6σ .

Acknowledgments

We are grateful for the extraordinary contributions of our PEP-II colleagues in achieving the excellent luminosity and machine conditions that have made this work possible. The success of this project also relies critically on the expertise and dedication of the computing organizations

that support *BABAR*. The collaborating institutions wish to thank SLAC for its support and the kind hospitality extended to them. This work is supported by the US Department of Energy and National Science Foundation, the Natural Sciences and Engineering Research Council (Canada), the Commissariat à l'Energie Atomique and Institut National de Physique Nucléaire et de Physique des Particules (France), the Bundesministerium für Bildung und Forschung and Deutsche Forschungsgemeinschaft (Germany), the Istituto Nazionale di Fisica Nucleare (Italy), the Foundation for Fundamental Research on Matter (The Netherlands), the Research Council of Norway, the Ministry of Education and Science of the Russian Federation, Ministerio de Ciencia e Innovación (Spain), and the Science and Technology Facilities Council (United Kingdom). Individuals have received support from the Marie-Curie IEF program (European Union), the A. P. Sloan Foundation (USA) and the Binational Science Foundation (USA-Israel).

-
- | | |
|---|---|
| <p>[1] I. I. Bigi, B. Blok, M. Shifman, and A. Vainshtein, Phys. Lett. B 323, 408 (1994); T. Browder, Proceedings of the 1996 Warsaw ICHEP Conference, edited by Z. Ajduk and A. K. Wroblewski, 1139, World Scientific (1997).</p> <p>[2] G. Buchalla, I. Dunietz, and H. Yamamoto, Phys. Lett. B 364, 188 (1995).</p> <p>[3] CLEO Collaboration, CLEO CONF 97-26, EPS97 337 (1997); T. E. Coan <i>et al.</i> (CLEO Collaboration), Phys. Rev. Lett. 80, 1150 (1998); R. Barate <i>et al.</i> (ALEPH Collaboration), Eur. Phys. Jour. C 4, 387 (1998).</p> <p>[4] B. Aubert <i>et al.</i> (BABAR Collaboration), Phys. Rev. D 68, 092001 (2003).</p> | <p>[5] B. Aubert <i>et al.</i> (BABAR Collaboration), Phys. Rev. D 75, 072002 (2007).</p> <p>[6] M. Zito, Phys. Lett. B 586, 314 (2004).</p> <p>[7] J. Charles <i>et al.</i>, Phys. Lett. B 425, 375 (1998); T. E. Browder, A. Datta, P. J. O'Donnell, and S. Pakvasa, Phys. Rev. D 61, 054009 (2000).</p> <p>[8] B. Aubert <i>et al.</i> (BABAR Collaboration), Phys. Rev. D 74, 091101 (2006).</p> <p>[9] J. Dalseno <i>et al.</i> (Belle Collaboration), Phys. Rev. D 76, 072004 (2007).</p> <p>[10] J. Brodzicka <i>et al.</i> (Belle Collaboration), Phys. Rev. Lett. 100, 092001 (2008).</p> |
|---|---|

- [11] B. Aubert *et al.* (BABAR Collaboration), Phys. Rev. D **77**, 011102 (2008).
- [12] T. Aushev, N. Zwahlen *et al.* (Belle Collaboration), Phys. Rev. D **81**, 031103 (2010).
- [13] B. Aubert *et al.* (BABAR Collaboration), Nucl. Inst. Meth. A **479**, 1 (2002).
- [14] D. J. Lange, Nucl. Instrum. Methods Phys. Res., Sect. A **462**, 152 (2001).
- [15] T. Sjostrand, S. Mrenna, and P. Skands, J. High Energy Phys. 05, 026 (2006).
- [16] S. Agostinelli *et al.* (GEANT4 Collaboration), Nucl. Inst. Meth. Phys. Res. Sect. A **506**, 250 (2003).
- [17] C. Amsler *et al.* (Particle Data Group), Phys. Lett. B **667**, 1 (2008) and 2009 partial update for the 2010 edition.
- [18] J. C. Anjos *et al.* (E691 Collaboration), Phys. Rev. D **48**, 56 (1993).
- [19] G. C. Fox and S. Wolfram, Nucl. Phys. B **149**, 413 (1979).
- [20] E. D. Bloom and C. Peck, Ann. Rev. Nucl. Part. Sci. **33**, 143 (1983).
- [21] H. Albrecht *et al.* (Argus Collaboration), Phys. Lett. B **241**, 278 (1990).
- [22] B. Aubert *et al.* (BABAR Collaboration), Phys. Rev. D **80**, 092003 (2009).
- [23] M. Pivk and F. R. Le Diberder, Nucl. Inst. Meth. A **555**, 356 (2005).

Appendix A: Fit PDF expressions

We give the expressions of the PDFs introduced in section IV (along with their parameters) and used to fit the m_{ES} distribution in the data.

1. Signal PDF

The signal PDF is given by:

$$\mathcal{P}_S(m_{ES}; m_S, \sigma_S, \alpha_S, n_S) = \begin{cases} \exp[-(m_{ES} - m_S)^2 / (2\sigma_S^2)] & m_{ES} > m_S - \alpha_S \sigma_S \\ \frac{(\frac{n_S}{\alpha_S})^{n_S} \exp(-\alpha_S^2/2)}{((m_S - m_{ES})/\sigma_S + \frac{n_S}{\alpha_S} - \alpha_S)^{n_S}} & m_{ES} \leq m_S - \alpha_S \sigma_S. \end{cases} \quad (\text{A1})$$

In this equation and in the following, we omit the factor that normalizes the PDF to unity.

2. Cross-feed PDF

The cross-feed PDF for modes containing no D^{*0} meson is described for the peaking part by:

$$\mathcal{P}_{CF}^{\text{peaking}}(m_{ES}; m_{CF}, \sigma_{CF}) = \exp[-(m_{ES} - m_{CF})^2 / (2\sigma_{CF}^2)]. \quad (\text{A2})$$

For modes containing at least one neutral D^* meson, the peaking component is described by:

$$\mathcal{P}_{CF}'^{\text{peaking}}(m_{ES}; m_{CF}, \sigma_{CF}, t_{CF}) = \exp \left[\frac{-\ln^2 \left(1 + t_{CF} \Lambda \frac{m_{ES} - m_{CF}}{\sigma_{CF}} \right)}{2 t_{CF}^2} - \frac{t_{CF}^2}{2} \right], \quad (\text{A3})$$

where $\Lambda = \sinh(t_{CF} \sqrt{\ln 4}) / (t_{CF} \sqrt{\ln 4})$. This function approaches a Gaussian function when the parameter t_{CF} vanishes.

The non-peaking part PDF is:

$$\mathcal{P}_{CF}^{\text{non peaking}}(m_{ES}; m_0, \xi_{CF}) = m_{ES} \sqrt{1 - (m_{ES}/m_0)^2} \times \exp[-\xi_{CF}(1 - (m_{ES}/m_0)^2)]. \quad (\text{A4})$$

3. Combinatorial background PDF

The combinatorial background PDF can be expressed as:

$$\mathcal{P}_{CB}(m_{ES}; m_0, \xi_{CB}) = m_{ES} \sqrt{1 - (m_{ES}/m_0)^2} \times \exp[-\xi_{CB}(1 - (m_{ES}/m_0)^2)]. \quad (\text{A5})$$

4. Peaking background PDF

The peaking background PDF is given by:

$$\mathcal{P}_{PB}(m_{ES}; m_{PB}, \sigma_{PB}) = \exp[-(m_{ES} - m_{PB})^2 / (2\sigma_{PB}^2)]. \quad (\text{A6})$$